CHALMERS

Influence of specimen geometry on fatigue crack growth rates in cast and forged Ti- and Ni-based alloys

Master's thesis in Applied Mechanics

TOBIAS MATTSSON

Department of Mechanics and Maritime Sciences
CHALMERS UNIVERSITY OF TECHNOLOGY
Göteborg, Sweden 2018

MASTER'S THESIS IN APPLIED MECHANICS

Influence of specimen geometry on fatigue crack growth rates in cast and forged Ti- and Ni-based alloys

TOBIAS MATTSSON

Department of Mechanics and Maritime Sciences
Division of Dynamics
CHALMERS UNIVERSITY OF TECHNOLOGY

Göteborg, Sweden 2018

Influence of specimen geometry on fatigue crack growth rates in cast and forged Ti- and Ni-based alloys
TOBIAS MATTSSON

Master's thesis 2018:34
Department of Mechanics and Maritime Sciences
Division of Dynamics
Chalmers University of Technology
SE-412 96 Göteborg
Sweden
Telephone: +46 (0)31-772 1000

Chalmers Reproservice
Göteborg, Sweden 2018

Influence of specimen geometry on fatigue crack growth rates in cast and forged Ti- and Ni-based alloys
Master's thesis in Applied Mechanics
TOBIAS MATTSSON
Department of Mechanics and Maritime Sciences
Division of Dynamics
Chalmers University of Technology

Abstract

Assuming linear elastic fracture mechanicsl two cracks with the same stress intensity factor will grow with the same rate, regardless of the geometry of the body. However, at GKN Aerospace test results from fatigue crack growth testing of C(T) and Kb specimens made from castings have shown distinct differences in fatigue crack growth rate where cracks in Kb specimens are growing faster than cracks in C(T) specimens. These observed differences have been studied and quantified. For fatigue crack growth test, cracked Kb specimens loaded in pulsating tension with $R = 0$ were growing 3.6 times faster than cracks in C(T) specimen, averaged over all test temperatures and the materials Ti-64, Ti-6242 and IN-718. New fatigue crack growth testing using C(T) specimens made from forged Ti-64 and IN-718 has been performed and compared to fatigue crack growth rates in Kb specimens made from forgings. The difference in fatigue crack growth rates between Kb and C(T) specimens made from forgings were found to be very small.

In order to investigate why cracks in Kb specimens made from castings are growing faster than cracks in C(T) specimens, the plastic zone size in Kb and C(T) specimens was evaluated through numerical simulations using the finite element method. Further, the grain sizes in cast Ti-64 and IN-718 specimens were measured. The measured grain sizes were found to be approximately 100 times greater in castings than in forgings. The investigations indicate that cracks in castings may be subjected to crack closure and further work aimed to measure the closure levels in Kb specimens compared to C(T) specimens is proposed.

Keywords: Fatigue crack growth, FCGR, T-stress, plastic zone size, LEFM, crack closure, Kb specimen, C(T) specimen

Preface

The work presented in this thesis has been carried out at the Division of Dynamics within the department of Mechanics and Maritime Sciences at Chalmers University of Technology and at the team for mechanical testing at GKN Aerospace Engine Systems in Trollhättan. Professor Anders Ekberg have been the supervisor and examiner from Chalmers and with Dr. Thomas Hansson as the supervisor at GKN Aerospace Engine Systems.

I would like to thank Dr. Thomas Hansson and Professor Anders Ekberg for all their help, guidance and encouragement throughout this process. I would also like to thank Dr. Sushovan Roychowdhury and Dr. Tomas Månsson at GKN Aerospce Engine Systems for their valuable input and guidance to this work. Moreover, I am very grateful for all help from Anders Oscarsson with measuring of grain sizes. Finally a great thank you to Karin Ericson and the mechanical testing team at GKN Aerospace Engine Systems for letting me carry this thesis out in a encouraging environment.

Trollhättan October 2018
Tobias Mattsson

Nomenclature

Abbrevations

ACR	Adjusted compliance ratio
CMOD	Crack mouth opening displacement
EDM	Electrical discharge machining
FCGR	Fatigue crack growth rate
FEM	Finite element method
LEFM	Linear elastic fracture mechanics
NASGRO	Fracture mechanics software suit
PM	Powder metallurgy
RT	Room temperature
SC01	Kb specimen in NASGRO
SIF	Stress intensity factor (also denoted K)
SS02	C(T) specimen in NASGRO
UTS	Ultimate tensile strength

Symbols

A	Actual life	
a	Crack depth for 2D crack geometries	mm
c	Crack width for 2D crack geometries	mm
f	Crack opening function	
K	Stress intensity factor (SIF)	$\mathrm{MPa}\sqrt{\mathrm{m}}$
K_{Ic}	Fracture toughness	$\mathrm{MPa}\sqrt{\mathrm{m}}$
$K_{\max}$	Maximum stress intensity factor during cycle	$\mathrm{MPa}\sqrt{\mathrm{m}}$
$K_{\min}$	Minimum stress intensity factor during cycle	$\mathrm{MPa}\sqrt{\mathrm{m}}$
K_{op}	Crack opening stress intensity factor	$\mathrm{MPa}\sqrt{\mathrm{m}}$
$\Delta K = K_{\max} - K_{\min}$	Range of stress intensity factor	$\mathrm{MPa}\sqrt{\mathrm{m}}$
ΔK_{th}	Threshold stress intensity factor	$\mathrm{MPa}\sqrt{\mathrm{m}}$
N	Number of cycles	Cycles
P	Predicted life	
$R = {}^{S_{\min}}/_{S_{\max}}$	Stress ratio	
S	Nominal stress	MPa
$S_{\max}$	Maximum nominal stress during cycle	MPa
$S_{\min}$	Minimum nominal stress during cycle	MPa

Greek letters

β	Biaxiality factor	
$\sigma_0 = {}^{(\sigma_y + \mathrm{UTS})}/_2$	Flow stress	MPa
σ_y	Yield stress	MPa

Test specimens

CN	Corner Notched
C(T)	Compact Tension
CCT	Center Cracked Tension
ESE(T)	Eccentrically Loaded Single Edge-Notched Tension
Kb	Kb bar, specimen with surface flaw
M(T)	Middle Tension
SENB	Single Edge Notched Bend
SENT	Single Edge Notched Tension

Contents

1 Introduction

Approximately ten years ago GKN was launching an extensive material testing program called the Themelio project. The objective was to compile a database of material properties to be used as design data for product development projects. One of these material properties was fatigue crack growth rates. GKN uses the Kb-bar specimen - which has a notched surface flaw- for testing of fatigue crack growth rates. For testing of the cast materials, concerns were raised that the coarse grain structure in cast material would lead to a spread of test results since the cracks in Kb specimens are relatively small compared to the grain size. This led to the decision to use both Kb specimens and standard C(T) specimens for fatigue crack growth testing in cast materials. When the data of the testing was evaluated one could see that there was a clear difference in fatigue crack growth rates between the Kb and C(T) specimens.

The growth of cracks in linear elastic bodies can be described by the use of linear elastic fracture mechanics, LEFM. When using LEFM the severity of a crack is described by the stress intensity factor range ΔK. In the expression for calculating ΔK there is a factor handling the geometry of the body in which the crack is located. The stress intensity range is used to predict how fast a crack will grow. Since the stress intensity range equation has this geometry factor a crack with a given stress intensity range is expected to grow with the same speed regardless of the geometry of the body.

Here the observed crack growth is contradicting the theory of LEFM: cracks in Kb specimens are observed to grow faster than cracks in C(T) specimens although they have same ΔK-value and by LEFM are expected to grow at the same rate. This contradiction is the the scoop of this thesis' work. The difference observed in fatigue crack growth rates between cracks in Kb and C(T) specimen will be examined and quantified. Possible reasons that can explain the observed differences will be studied and evaluated. This is done by a literature survey and further investigations of phenomena affecting the rate of crack growth.

1.1 Objective

The objective of this thesis is to

- Document and quantify the observed differences in crack growth rates in Kb specimens compared to C(T) specimens.
- Study how the test specimen geometry influences the fatigue crack growth test results.

1.2 Limitations

The work is limited to include and consider the following areas

- Cast and forged material of titanium Ti-64 and Ti-6242 and the nickel based material Inconel-718, IN-718.
- Crack propagation in C(T) and Kb bar test specimens.
- Fatigue crack growth rate in region II, where crack growth can be described by Paris law.
- Temperature ranging from 22°C to 650°C

1.3 GKN Aerospace

This thesis has been carried out within the team for mechanical testing at GKN Aerospace Engine Systems in Trollhättan, Sweden, here called GKN. GKN are manufacturing and developing components for jet and rocket engines. GKN components can for example be found in Airbus A380, A350 and A320neo and in Boeing 747, 787 and 737MAX. The RM12 jet engine for the Swedish multirole fighter aircraft JAS 39 Gripen is develooped, manufacctured and maintained by GKN.

1.4 Contributions

All worked reported have been performed by the author with the following exceptions

- Evaluation and testing of the fatigue crack growth rates in castings using Kb and C(T) specimens. This work have been performed by GKN Aerospace before the work with this thesis were started.
- Mechanical testing of the fatigue crack growth rates in forgings using C(T) specimens. The tests were initiated by the author, likewise where the test conditions set by the author. The mechanical testing and evaluation were carried out by Metcut Research Inc.
- Measuring of grain sizes. All steps in the procedure to measure the grain size in castings have been carried out by Anders Oscarsson. The author attended all steps in order to gain knowledge of the process and in order to understand the results.

2 Theory

2.1 Fracture mechanics

In a cracked body of an isotropic linear elastic material the stress is approaching infinity near the crack tip. By defining a polar coordinate system at the crack tip can the stress distribution be written as

$$\lim_{r\to 0} \sigma_{ij} = \frac{K}{\sqrt{2\pi r}} f_{ij}(\theta) \tag{2.1}$$

where K is the *stress intensity factor*, r is the distance from the crack tip and f_{ij} is a geometry factor. Since the stress is approaching infinity, K is used to describe the severity of the crack. In general, K can be expressed as

$$K = FS\sqrt{\pi a} \tag{2.2}$$

where a is the crack length, F is a dimensionless geometry factor and S the nominal applied stress. For a more formal definition see [1–4].

Equation (2.1) is based on a infinite power series which produces a $1/\sqrt{r}$ singularity at the crack tip. In linear elastic fracture mechanics, LEFM, equation (2.1) is the only term of the power series included in the expression of the stress distribution as all other terms vanish as $r \to 0$ or are assumed to be small compared to the singular term. However, the second term in the power series is not approaching zero at the crack tip, instead it remains finite and can in some applications has significant influence on the stress distribution. This second terms is often referred to as the *T-stress*. If included, equation (2.1) is extended to (cf [1, 2])

$$\sigma_{ij} = \frac{K}{\sqrt{2\pi r}} f_{ij}(\theta) + T_{ij} \tag{2.3}$$

For LEFM to be valid in test specimens, the uncracked ligaments of the test specimen have to be greater than a certain value which is based on the maximum stress intensity factor and the yield stress of the material. In the ASTM standard for measurement of fatigue crack growth rates [6] and in Dowling [3] is that defined as

$$W - a \geq \frac{4}{\pi}\left(\frac{K}{\sigma_y}\right)^2 \tag{2.4}$$

where $W - a$ is the uncracked ligament, K the stress intensity factor and σ_y the yield stress.

2.2 Fatigue crack growth

The average crack growth per cycle for a number of cycles is called the fatigue crack growth rate, FCGR, and is denoted da/dN. The FCGR is measured as a function of the stress intensity range ΔK which based on equation (2.2) is defined as

$$\Delta K = F\Delta S\sqrt{\pi a} = F(S_{\max} - S_{\min})\sqrt{\pi a} \tag{2.5}$$

where $S_{\max}$ and $S_{\min}$ are the maximum and minimum applied nominal stress respectively. The geometry factor F for simple crack geometries is to be found in handbooks such as [1, 4].

If the FCGR is plotted versus the stress intensity range in log–log scale, one can divide the crack growth into three regions, as seen in Figure 2.1. In region I the FCGR is approaching zero as $\Delta K \to \Delta K_{\text{th}}$, where ΔK_{th} is the *fatigue crack growth threshold*, meaning the lowest stress intensity range that gives crack growth. In the second region the logarithm of the crack growth is linearly dependent on $\log \Delta K$ in the log-log plot. The growth can be expressed by Paris law which is defined as

$$\frac{da}{dN} = C\left(\Delta K\right)^m \tag{2.6}$$

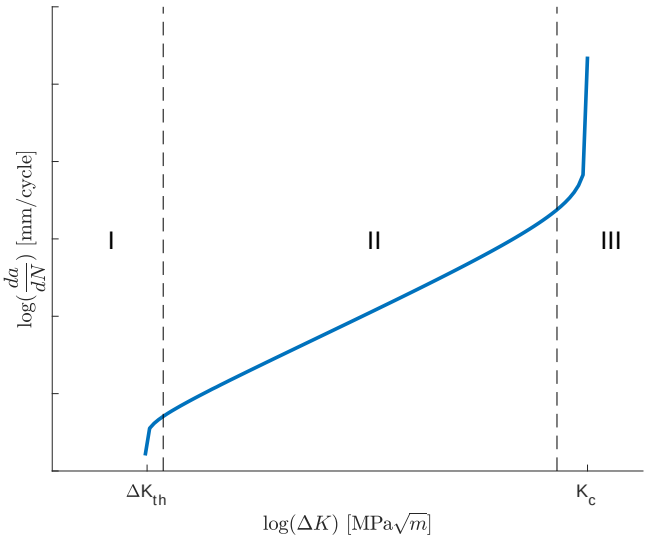

Figure 2.1: *Fatigue crack growth rate regions*

At higher growth rates in region III the FCGR is approaching infinity as $\Delta K \rightarrow K_{Ic}$ where K_{Ic} is the *fracture toughness* which is the stress intensity leading to catastrophic failure.

For a given set of test conditions, *stress ratio* $R = \frac{S_{\min}}{S_{\max}}$, temperature and material, Paris law is describing the crack growth in the second region. Paris law was proposed by Paul Paris in the 1960s [3]. In later years more involved models that can include all three regions (cf. Figure 2.1) and also include the influence of the stress ratio have been developed. One such equation is the NASGRO-equation used in the software with the same name, (cf. Figure 2.1). The NASGRO equation is described in the NASGRO manual, [5], and is defined as

$$\frac{da}{dN} = C\left[\left(\frac{1-f}{1-R}\right)\Delta K\right]^n \frac{\left(1-\frac{\Delta K_{\text{th}}}{\Delta K}\right)^p}{\left(1-\frac{K_{\max}}{K_c}\right)^q} \tag{2.7}$$

where f is the crack opening function for plasticity induced crack closure, which is the relation between the stress intensity when the crack is first fully open, K_{op}, and the maximum applied stress intensity $K_{\max}$. The value of the crack opening function is in NASGRO estimated by equation (2.8) and (2.9)

$$f = \frac{K_{\text{op}}}{K_{\max}} = \begin{cases} \max\left(R, A_0 + A_1 R + A_2 R^2 + A_3 R^3\right) & R \geq 0 \\ A_0 + A_1 R & -2 \leq R < 0 \end{cases} \tag{2.8}$$

$$\begin{aligned} A_0 &= \left(0.825 - 0.34\alpha + 0.05\alpha^2\right)\left[\cos\left(\frac{\pi}{2}\frac{S_{\max}}{\sigma_0}\right)\right]^{1/\alpha} \\ A_1 &= \left(0.415 - 0.071\alpha\right)\frac{S_{\max}}{\sigma_0} \\ A_2 &= 1 - A_0 - A_1 - A_3 \\ A_3 &= 2A_0 + A_1 - 1 \end{aligned} \tag{2.9}$$

where $\frac{S_{\max}}{\sigma_0}$ is the relation between the maximum nominal applied stress and the flow stress, σ_0. The flow stress is defined as the mean value of the yield stress, σ_{y}, and ultimate tensile stress, UTS. The parameter α is a constraint factor ranging from 1 for plane stress condition to 3 for plane strain.

2.3 FCGR testing

In order to find values of the parameters in the equations describing the crack growth, material testing has to be performed. The testing is done by cyclically loading test specimens in well controlled environments and recording essential test values, such as crack length, applied load, temperature and cycle number. From the test data the FCGR can be calculated as well as the stress intensity range. How to conduct a FCGR test is described in ASTM E647, [6]. Before the sampling of test data is started the specimen is pre-cracked. This is done since the models used for fatigue crack growth are based on the assumption of a perfect crack, i.e a crack without a tip radius. This assumption is not true for machined notches and therefor the specimen is pre-cracked. After the crack has grown to a predetermined crack size the sampling is stopped, and the specimen is loaded in tension until it breaks, this is called final rupture and is done to be able to inspect the fracture surfaces and optically measure crack lengths. The last crack length recorded before final rupture is called final crack length.

2.3.1 Test specimens

There exists a number of specimen geometries used for FCGR testing where the compact specimen C(T) loaded in tension is the most used one. Other specimens can be loaded in bending or biaxially, and the crack can grow in one direction or extend along a plane. At GKN the so-called Kb specimen is mostly used. This is a surface flaw specimen with a crack growing in in a plane forming a half circular/elliptical crack. For testing of castings, GKN has also used the C(T) specimens.

C(T)-specimen

The C(T)-specimen used at GKN can be seen in Figure 2.2. The crack in C(T)-specimens is growing in one direction and the crack front is assumed to be straight through the thickness of the specimen. The length of the crack is measured from the center of the holes and is normally denoted a, in NASGRO the crack length is denoted c as seen in Figure 2.4a. The crack size can be measured with several different techniques, for example by marking length scales on the sides of the specimen and measure the crack size through a microscope. Crack growth is monitored by the CMOD method where the displacement over the opening of the specimen is measured and converted to crack length, or by the potential drop method, described in the Kb specimen section below. Through the holes in the specimens the load is applied perpendicular to the crack plane.

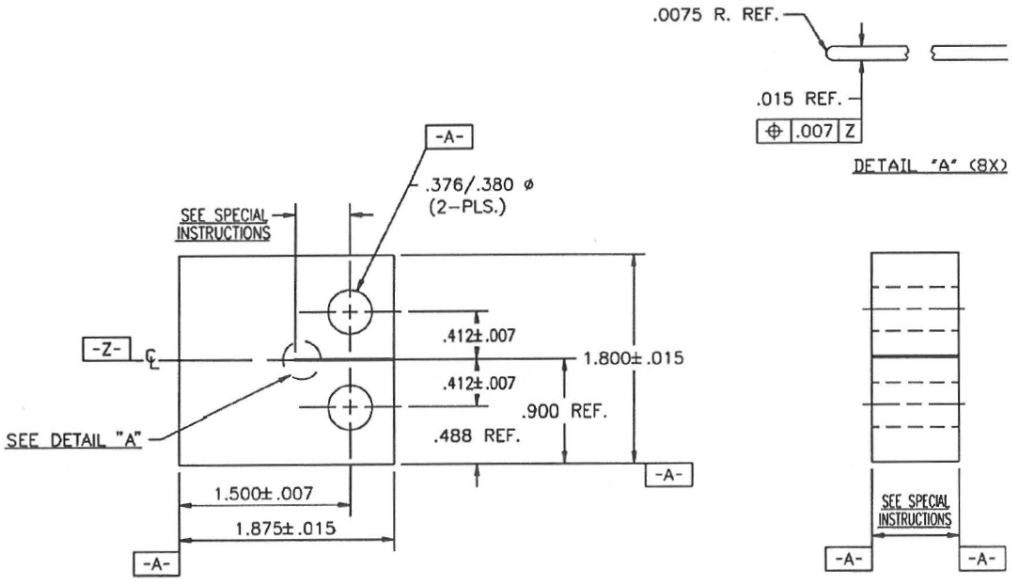

Figure 2.2: *C(T)-specimen, dimensions in inches. The specimen width at GKN is 6.35mm.*

Kb specimen

The Kb-specimen is a surface flaw specimen where the crack is growing in a plane. The size of the crack is measured in two directions, a and c. The a-direction is measured through the thickness of the specimen whilst the c measure is half the length of the crack at the surface of the specimen, as indicated in Figure 2.4b. The crack is initiated from the notch, placed at the surface of the specimen. The notch is made by electrical discharge machining, EDM. In Figure 2.3 the Kb-specimen used at GKN is shown.

At GKN the size of the crack is measured by the potential drop (PD) method, combined with measurements of the pre- and final crack. The pre- and final cracks is marked on the fracture surfaces by heating the specimen to a specific temperature which is held over some time. The increased temperature oxidizes the surface, giving the surface a different color. By combing different temperatures and hold times, the fracture surface can be given different colors. This method is called heat-tinting and leaves areas with different colors that can be measured in a microscope after testing. In the PD-method a direct current at a constant level is applied through the specimen. When the crack grows the resistance of the specimen is increasing and thereby the electrical potential. The electrical potential over the crack is measured throughout the test and is "translated" into crack size by a calibration curve and the measures of the pre- and final crack sizes, cf. [7]. At GKN the PD-method is used to predict the crack size in between the measured pre- and final crack lengths.

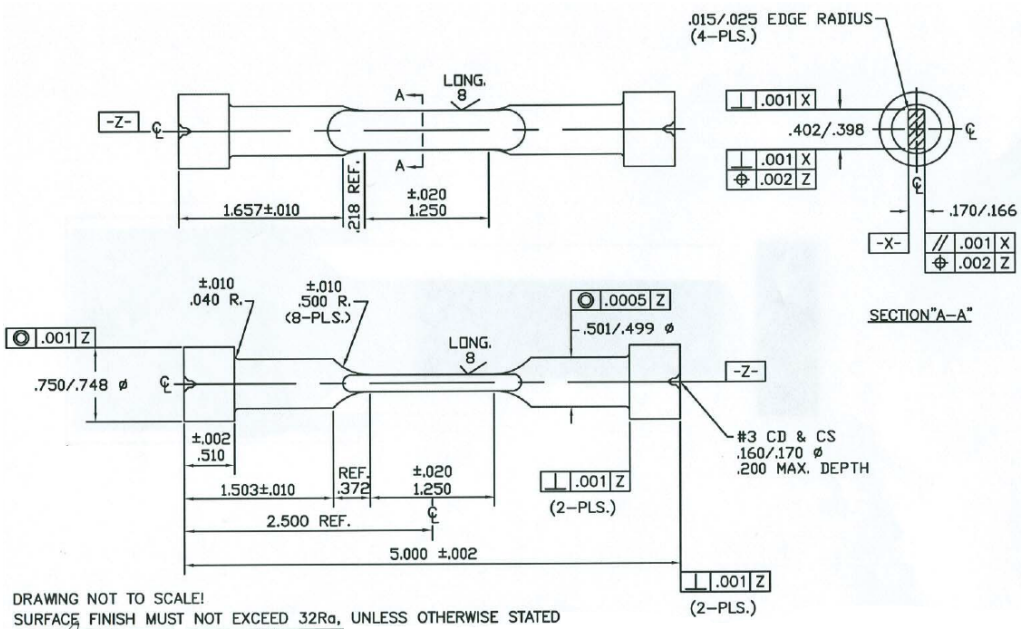

Figure 2.3: *Kb-specimen, dimensions in inches.*

2.3.2 Test evaluation

The raw test data have to be translated to ΔK values and matched to corresponding da/dN values. The stress intensity factor range is calculated from the applied load and the geometry of the specimen according to equation (2.5), or by use of the NASGRO software. The geometry factor F is found in handbooks, such as [4]. As part of the evaluation the LEFM validity according to equation (2.4) has to be checked. ASTM E647 [6] defines two methods to calculate the FCGR: the secant method or the incremental polynomial method. At GKN the secant method is adopted and the FCGR is approximated as

$$\left(\frac{da}{dN}\right)_i = \left(\frac{\Delta a}{\Delta N}\right)_i = \frac{a_{i+1} - a_i}{N_{i+1} - N_i} \tag{2.10}$$

where i denotes a sampling point. The polynomial methods includes fitting the data points to a second order polynomial which reduces the data scatter. The measured data points are then fitted to a fatigue crack growth model, i.e Paris law, with the least square fit method, cf. [8].

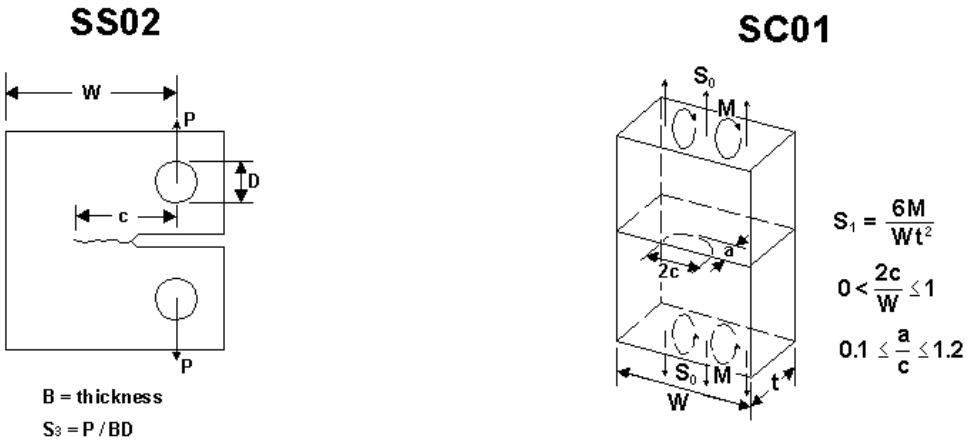

(a) *C(T) specimen NASGRO* **(b)** *Kb specimen in NASGRO*

Figure 2.4: *Test specimens in NASGRO*

3 Literature survey

There is no consensus in the literature whether the geometry of the test specimen can influence the crack propagation. Some authors reports that a geometry influence can be observed and linked to the magnitude of the T-stress. The reports of in which types of specimens cracks are growing fast or slow are however not consistent. Here some mechanisms and theories effecting the crack growth rates are presented. These include the influence of the T-stress, plastic zone and crack closure.

3.1 T-stress

In Suresh [2, p152], the T-stress is included in the description of the stress state at the crack tip. Suresh reports that in most cases of LEFM applications it is sufficient to omit the T-stress, but doing so can induce significant errors for example in cases of short cracks. Anderson [1, p160] is also introducing the T-stress and the biaxiality ratio β, which for mode I load is defined as

$$\beta = \frac{T\sqrt{\pi a}}{K} \tag{3.1}$$

where T is the T-stress, a the crack length, and K the mode I stress intensity factor. Anderson reports that CC(T)[1] specimens have a biaxiality ratio of $\beta = -1$, since CC(T) specimens have a geometry factor close to one for small cracks, [1, 3], the T-stress becomes $T = -S$, where S is the nominal stress applied to the specimen.

Hutăr et al. [9, 10] present a difference in fatigue crack growth for C(T) and CC(T) specimens, where the growth rates in CC(T) specimen are greater than for C(T) specimens. The differences are based on their own testing and by referring to other sources. The material that they worked with was a carbon steel. They say that C(T) specimens represent a high level of constraint and positive T-stresses, while the CC(T) specimens have a low level of constraint and negative T-stresses. By calculating the plastic zone size with the modified boundary layer method using ANSYS, they where able to derive an effective stress intensity factor $K^{\text{eff}} = \lambda K$, were $\lambda = \lambda\left(\frac{T}{\sigma_y}\right)$. When they plotted their test data in a $da/dN - \Delta K^{\text{eff}}$ plot, the difference in fatigue crack growth rates was more or less eliminated.

Jie Tong [11] is reporting discrepancies between C(T) and CN[2] specimens for Waspaloy at 650 °C as well as for the PM alloy U720Li at RT. In both cases the C(T) specimens have a greater crack growth rate than the CN specimens. Tong also reports that fatigue life prediction of a gas turbine disc, based on test data from CN specimens more precisely predicts the life than predictions based on C(T) specimen data. The ratios of actual life to predicted life (A/P) is reported to be 0.94 for predictions based on CN specimen data whilst the same ratio is 0.48 for predictions based on C(T) specimen data. Tong was performing tests on C(T), SEN(T)[3] and CC(T) specimens and found (in contradiction to, and as mentioned in Hutăr et al.) that C(T) specimens predicts higher crack grows rates than both CC(T) and SEN(T) specimens. It is suggested that the T-stress can explain the discrepancy but a $da/dN - \Delta K$ plot is not provided. Instead a normalized value of the T-stress for the different specimen types is presented.

In [12] Varfolomeev et al. compare crack propagation rates for C(T), M(T)[4], round and rectangular surface flaw specimens for the steel EA4T. The round surface flaw specimens is called BP2 and the rectangular specimen is called BP3. Both surface flaw specimens are loaded in bending. The data from C(T) and M(T) specimens are collected from literature while the surface flaw testing is performed as part of the study. They conclude that C(T) and M(T) specimens have the greatest differences in crack growth rates among the specimens in their study. Cracks in M(T) specimens are reported to grow twice as fast as cracks in C(T) specimens in the interval of $\Delta K = 12 - 20\,\text{MPa}\sqrt{\text{m}}$. Thus, surface flaw specimens are found to grow faster than C(T) specimens in

[1] Center Crack Tension. Plate with a through thickness crack loaded in tension. Load is applied perpendicular to the width of the crack, cf. [1]

[2] Corner Notched. Rectangular or quadratic bar loaded in tension with a notch in a corner. 2 dimensional crack forming a quarter circle.

[3] Single Edge Notched Tension. Rectangular or quadratic bar loaded in tension, notched on one side.

[4] Middle Tension. Cf. CC(T)

Varfolomeev's study. The difference in growth rate seems to be less than in previous cited papers. Varfolomeev et al. [12] compiles T-stress results from literature for the four specimen included in their study and present the results using the biaxiality factor β. The biaxiality factor for the rectangular surface flaw specimen is reported to be approximately -1, whilst the biaxiality factor for C(T) specimens ranges from 0.15 to 0.6, depending on the crack size. Varfolomeev et al. do not consider the correlation between the difference in crack growth rates and biaxiality factor to be high. Instead they believe that the crack tip plasticity is affecting crack growth and propose that the normalized plasticity parameter L_{r} could be used to show the geometry influence of the specimen. They define the plasticity parameter as

$$L_{\mathrm{r}} = \frac{P}{P_{\mathrm{L}}} = \frac{\sigma_{\mathrm{ref}}}{\sigma_y} \tag{3.2}$$

where P is the applied load, P_{L} is the associated plastic limit load, σ_{ref} is a reference stress and σ_y the yield stress.

3.2 Plastic zone size

The plastic zone at the crack tip can be estimated as [1–3]

$$\begin{aligned} r_p &= \frac{1}{3\pi}\left(\frac{K_I}{\sigma_y}\right)^2 \qquad \text{Plane strain} \\ r_p &= \frac{1}{\pi}\left(\frac{K_I}{\sigma_y}\right)^2 \qquad \text{Plane stress} \end{aligned} \tag{3.3}$$

Dowling discusses that yielding at the crack tip leads to larger deformation which gives an even greater plastic zone. This fact is included in the estimation of the plastic zone size in equation (3.3) and motivated by Anderson in [1]. This enlargement of the plastic zone due to larger deformation is not accounted for in [13] where the plastic zone size is given as

$$r_p = \frac{1}{2\alpha\pi}\left(\frac{K}{\sigma_y}\right)^2 \tag{3.4}$$

Where α indicates the stress state, $\alpha = 1$ represents plane stress and $\alpha = 3$ plane strain.

Suresh [2] is presenting the work by Dugdale in 1960 where he estimated the plastic zone for a thin plate loaded in plane stress as

$$r_p = \frac{\pi}{8}\left(\frac{K_I}{\sigma_y}\right)^2 \tag{3.5}$$

Camas [14] performed a finite element analysis for C(T) specimens and found that the plastic zone size at the surface of the specimen is approximately of the same size as in the center of the specimens. This contradicts the classical presumption of a dog bone shaped plastic zone along the crack front. In Figure 3.1 the results of Camas' study for a 6mm wide C(T) specimen are presented. It is seen that the location of the largest plastic zone along the crack front varies with the applied stress intensity factor.

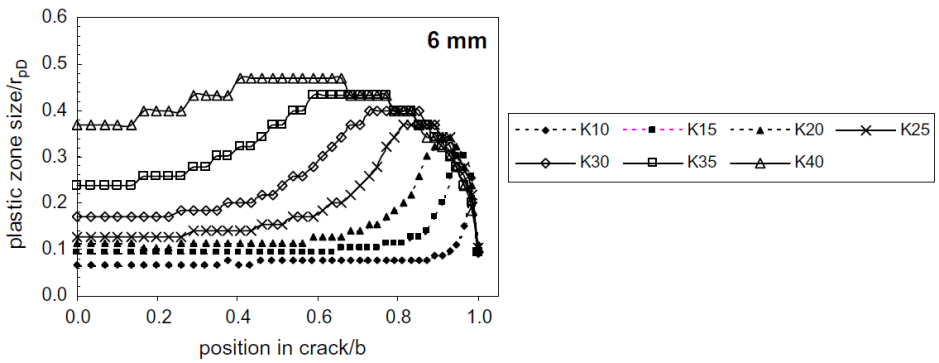

Figure 3.1: *Plastic zone size scaled with the plastic zone size estimation by the Dugdale method, from the symmetry plane to the free surface. The specimen is a C(T) specimen, width = 6mm. Kxx indicates the applied stress intensity. [14]*

3.3 Crack closure

Studies shows that a crack can close before the remotely applied load goes into compression [15]. This phenomenon is called crack closure. It is argued that the crack only can grow when it is fully open, cf.[2, p228]. From this can one define an effective stress intensity factor, ΔK_{eff}, that drives the crack propagation, as

$$\Delta K_{\text{eff}} = K_{\max} - K_{\text{op}} \tag{3.6}$$

where K_{op} is the stress intensity factor when the crack is fully open. Suresh [2, p223] proposes that crack closure can arise from five different sources:

1. **Plasticity induced crack closure**, is due to residual stresses behind the crack tip. These residual stresses arise when the crack is growing through the plastic zone, hence the name.

2. **Oxide induced crack closure** is when the crack is wedged by a thick oxide layer on the fracture surfaces.

3. **Roughness induced crack closure** is most likely to occur when the plastic zone is smaller than the grain size and is due to serrated and faceted fracture surfaces.

4. **Viscous induced crack closure** occurs when oil or water effects the crack growth

5. **Phase transformation induced crack closure**. If phase transformation occurs at the crack tip, it can induce crack closure in the same way as plasticity induced crack closure.

Rembeck and Sjöblom [16] studied plasticity induced crack closure in Kb specimens by FEM analysis and showed that the closure function $f = \frac{K_{op}}{K_{max}}$ is approximately 0.3 for $R = 0$ and 0.6 for $R = 0.5$ in cast IN-718 at both room temperature and at 650°C. This means that the the closure effect occurs also at $R = 0.5$, since $K_{op} = 0.6K_{max} > K_{min} = 0.5K_{max}$.

Suresh [2, p235] reports discrepancies of crack closure/opening stresses through the thickness of thick center cracked plates. The T-stress is said to be able to explain these discrepancies. He also reports that discrepancies of crack closure depending on the specimen geometry have been seen. Introduction of the T-stress has less significance in plane stress than in plane strain. Plane strain is reported to result in less crack closure than plane stress conditions.

Lundström [17] is presenting a modified Paris law where the stress ratio as well as the closure function f (see equation (2.8)) introduced by Newman and used in for example the NASGRO equation is included.

$$\begin{aligned} \frac{da}{dN} &= C\left(\Delta K_{\text{eff}}\right)^n \\ &= C\left(K_{\max} - K_{\text{op}}\right)^n \\ &= C\left(\frac{1-f}{1-R}\Delta K\right)^n \end{aligned} \tag{3.7}$$

Ball et al. [18] state that studies have shown that a crack seems to grow before the crack is fully open, i.e for $K < K_{\text{op}}$. They say that if the effective stress intensity factor ΔK_{eff} is calculated from the adjusted compliance ratio (ACR) this effect can be eliminated. The ACR is defined as

$$\text{ACR} = \frac{\Delta\delta_{\text{eff}} - \Delta\delta_i}{\Delta\delta_{\text{app}} - \Delta\delta_i} = \frac{C_{\text{S}} - C_i}{C_{\text{o}} - C_i} \tag{3.8}$$

where $\Delta\delta_{\text{eff}}$, $\Delta\delta_{\text{app}}$ and $\Delta\delta_i$ are the actual (measured), the closure free and the uncracked displacement ranges respectively, whilst C_{S}, C_{o} and C_i are secant, closure free and uncracked compliances respectively. Using the ACR method the effective stress intensity range is defined as

$$\Delta K_{\text{eff}} = \text{ACR} \cdot \Delta K_{\text{app}} \tag{3.9}$$

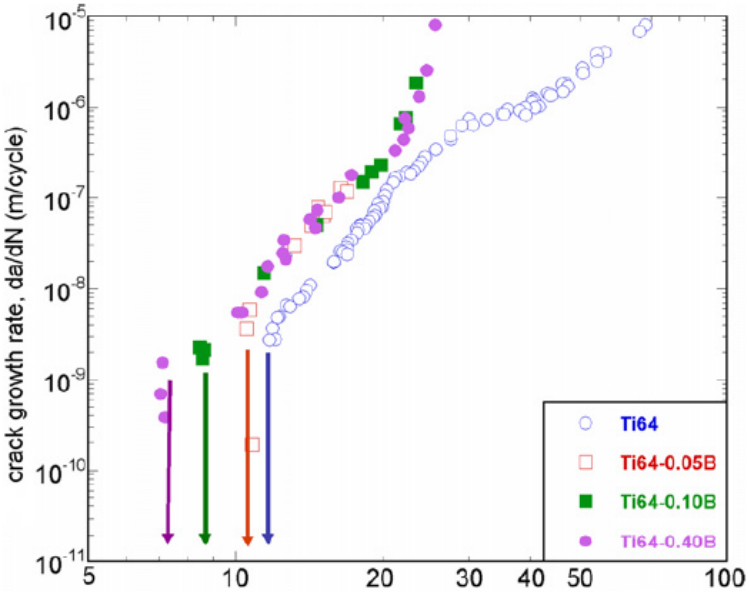

Figure 3.2: *Fatigue crack growth testing results in cast Ti-64 with addition B, compared to literature data for fatigue crack growth in cast Ti-64 without B addition. [20]*

3.4 Literature on crack propagation data

Forman and Mettu in [19] were investigating the influence of specimen geometry and crack type and derived material data for both fracture toughness and crack propagation in a bar from Ti-64. They used data from C(T) and SEB[5] specimens as the reference and compared to a range of other specimen types, including a specimen with a surface flaw in a rectangular bar, i.e more or less a Kb specimen. Forman and Mettu concluded that *"Fatigue crack growth rates from standard specimens can be used with reasonable accuracy in the case of surface and corner cracks"*. When comparing Forman's and Mettu's data of fatigue crack growth rates in Kb specimens to the GKN data of forged Ti-64 from Kb specimens no major difference is found.

3.5 Influence of microstructure

Sen et al. [20] examined the influence of adding Boron (B) to Ti-64 casts and conclude that addition of B is refining the micro structure of the alloy. In cast Ti-64 without B addition Sen et al. measured the grain size to 1.700 mm, with 0.05 wt% addition of B to the material the grain size was reduce to 0.233 mm. When the B fraction was further increased the grain size was even more refined, but not as pronounced as from 0 to 0.05 wt%. At 0.4 wt% B addition were the grain size measured to be 0.139 mm. They conducted fatigue crack growth testing of the Ti-64 with B addition, and compared it with literature data of fatigue crack growth rates of cast Ti-64 without B addition, cf. Figure 3.2. The addition of B to cast Ti-64 gave an increase in fatigue crack growth, but the weight fraction of B addition did not affect the fatigue crack growth.

[5]Single Edge Bend. Same as SEN(T), but loaded in bending.

4 Investigations of crack propagation

4.1 Quantification of discrepancies

The difference in fatigue crack growth rates between Kb and C(T) specimens made from castings are documented at GKN by Delin [21] by plotting two NASGRO curves for each material, temperature and R-ratio. One of the curves was fitted from Kb test specimen data whilst the other was fitted from C(T) test specimen data. From this documentation it could be seen that there is a difference in fatigue crack growth rate, FCGR, between Kb and C(T) specimens, where cracks in Kb specimens are growing faster than in C(T) specimens. In order to quantify the difference and to investigate if the difference can be seen in raw test data as well as in the numerical predictions (NASGRO and or Paris curve) the raw data was plotted along with two Paris curves, one fitted to Kb specimen test data and one fitted to C(T) specimen test data. The parameters in the Paris curves were evaluated by linear regression.

In order to quantify discrepancies, two different methods were used. The first was simply to compare the FCGR predicted by Paris law for a given ΔK value. The second method was to compare the actual life for a specific test specimen with an estimated life for the same specimen.

4.1.1 Fatigue crack growth rate

Since the Paris law parameters were determined separately for the C(T)-data and the Kb-data, two different fatigue crack growth values can be evaluated for a given ΔK value. This was done in order to quantify how much faster a crack is predicted to grow in the Kb specimen as compared to the C(T) specimen. The fatigue crack growth rates were compared at $\Delta K = \Delta K_{\text{mid}}$, where ΔK_{mid} is defined as

$$\log\left(\Delta K_{\text{mid}}\right) = \frac{\log\left(\max\left[\min\left(\Delta K_{\text{Kb}}\right), \min\left(\Delta K_{\text{C(T)}}\right)\right]\right) + \log\left(\min\left[\max\left(\Delta K_{\text{Kb}}\right), \max\left(\Delta K_{\text{C(T)}}\right)\right]\right)}{2} \tag{4.1}$$

where ΔK_{Kb} and $\Delta K_{\text{C(T)}}$ are all ΔK data points for the Kb and C(T) specimens respectively. With this definition, ΔK_{mid} is the logarithmic mean point of the interval where test data from both Kb and C(T) specimens are available. Since the ΔK interval of test data depends on the test parameters (material, temperature and R-ratio) is a unique ΔK_{mid} determined for each set of test parameters.

Figure 4.1 compares crack growth in C(T) and Kb specimens for Ti64 at room temperature (RT) and at $R = 0$. In the figure ΔK_{mid} is marked with a black cross on each Paris curve. The crosses are connected with a black solid line. Plots for all materials, temperatures and R-ratios can be seen in Appendix A. In Figure 4.1 it is seen that the data points from Kb specimens are separated from more or less all C(T) specimen points, with the Kb data points located above the CT data points, i.e cracks are growing faster in Kb specimens than in C(T) specimens.

Table 4.1 compiles results from the comparison, with all relations between crack growth rates in Kb and C(T) specimens presented. The greatest difference is found for Ti-6242 at room temperature and $R = 0$. Here the Kb specimen cracks are growing 6.3 times faster than cracks in the C(T) specimens. For IN-718 at 400°C and $R = 0.5$ the difference is the least with cracks in the Kb specimens growing 1.8 times faster than the in C(T) specimens. Table 4.1 contains data from 26 unique material, temperature and load level combinations, and the Kb specimen cracks are consistently growing faster than C(T)-specimens. For $R = 0$, cracks in Kb specimens are on average growing 3.6 times faster than cracks in C(T) specimens whilst for $R = 0.5$ cracks in Kb specimens are on average growing 3.2 times faster than cracks in C(T) specimens.

4.1.2 Actual versus predicted life

A great part of a components life regarding crack propagation relates to low ΔK values. This means that comparing the FCGR at a fixed ΔK value can give somewhat misleading information. So as a complement to the quantification above, the actual lives for some test specimens were compared to a predicted life. The

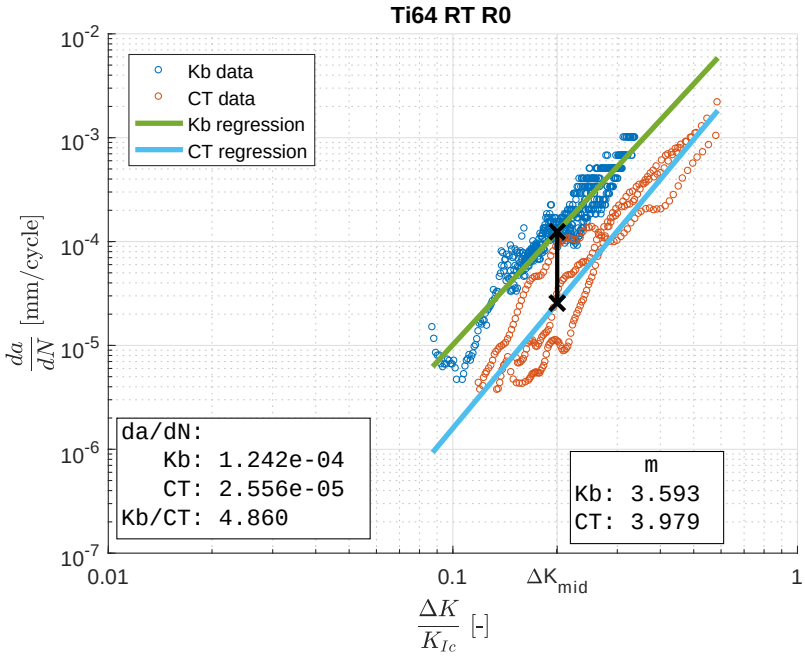

Figure 4.1: *Fatigue crack growth of cast Ti-64 in CT specimens compared to Kb specimens.*

Table 4.1: *Fatigue crack growth rates for Kb specimens compared to fatigue crack growth rates for C(T) specimens. The table shows how much faster a crack is estimated to grow in a Kb specimen as compared to a C(T) specimen.*

	Ti-64				Ti-6242				IN-718				
Temperature [°C]	RT	150	250	350	RT	250	350	450	RT	400	550	600	650
$R = 0$	4.9	4.4	2.2	3.8	6.3	3.6	4.4	3.3	3.8	2.9	2.7	2.4	2.4
$R = 0.5$	3.9	4.4	3.3	2.5	4.3	3.5	3.0	2.4	2.2	1.8	3.0	3.7	3.6

actual life was taken from test reports and the prediction of fatigue life was computed using NASGRO 8.21. This investigation was performed only for Ti-64 at RT and $R = 0$, and all life predictions were done using a NASGRO curve fitted to Kb specimen data. Life prediction analyses were performed for three C(T) specimens and four Kb specimens. FCGR tests were done for four C(T) specimens, but one specimen gave no valid data points due to crack deviation. For life prediction of C(T) specimens the SS02 model was used, cf. Figure 2.4a, whilst the SC01 model was used for Kb specimens, cf. Figure 2.4b. Geometry and load data used in NASGRO were taken from the test reports for the specimen in question.

The results are shown in Table 4.2 where the actual life is divided by the predicted life, A/P. It is found that for the C(T)-specimens the actual life is at least 3.56 times longer than the predicted life. This is in line with results from comparing FCGR, since the cracks in Kb specimens are growing faster than in C(T) specimens. Thus, the estimated life for C(T) specimens will be shorter than the actual life if a Kb specimen based data model is used. The results for Kb specimen are also presented as a method verification. Since the life prediction employs data from the Kb specimens, actual lives and predicted lives should be similar for Kb specimens.

Table 4.2: *Actual life compared to estimated life for Ti-64 at RT and $R = 0$ with crack growth parameters fitted to Kb specimen data.*

Specimen	CT1	CT2	CT3	Kb1	Kb2	Kb3	Kb4
A/P	6.42	8.56	3.56	1.12	0.89	1.14	1.14

4.2 Influence of measured crack length and evaluation method for Kb specimens

In the evaluation procedure the crack lengths in the a and c direction are measured using a microscope. The crack lengths are measured at pre-crack and final crack length. Since the fracture surface in a cast specimen is very rough it can be hard to accurately determine the crack length, and the results can depend on who performed the measurements. To investigate the influence of the measured crack size, the evaluation procedure was redone for two Ti-64 specimens, (Kb1 and Kb33). Firstly, the crack sizes were measured once more and the results were compared to previous measurements. From this set of measurements a worst case scenario for each specimen was defined, meaning, the largest pre-crack size measured was paired with the smallest measured final crack. This combination will give the slowest possible crack growth for a Kb specimen. Using this worst case scenario measurements of crack lengths, the evaluation of fatigue crack growth rates and stress intensity factors were redone. The re-evaluation was performed using three slightly different methods. The first evaluation method used was the method currently used at GKN, the second evaluation method used was based on the work in [7] and is the same as the currently used method except that a more advanced calibration curve is used for the PD-method. Lastly, an older evaluation method was used, were the depth to width ratio a/c of the crack was assumed to be one.

In Figure 4.2 the results from the re-evaluation are presented along with the calculated fatigue crack growth before re-evaluation. This is compared to the fatigue crack growth rate for C(T) specimens in the same material and at the same temperature and stress ratio. It is seen that the re-evaluation has shifted the fatigue crack growth in Kb specimens towards the fatigue crack growth rates in C(T) specimens. The shift is more pronounced for Kb specimen Kb33; which probably is due to a larger difference in measured crack sizes than for specimen Kb1.

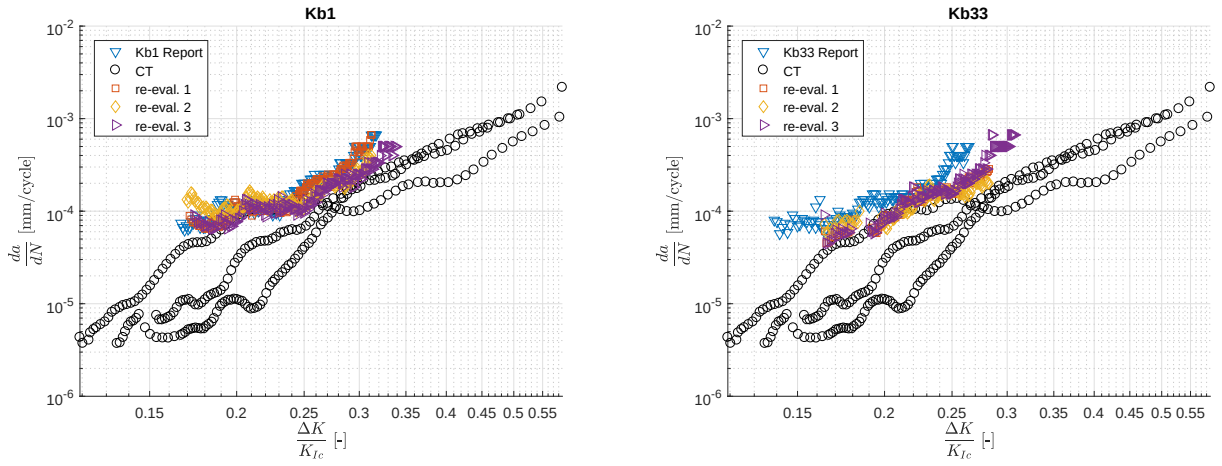

(a) *Kb specimen Kb1* **(b)** *Kb specimen Kb33*

Figure 4.2: *Re-evaluation of Kb specimens in Ti-64 at RT and* $R = 0$

4.3 Crack growth evaluation using NASGRO

In order to investigate how NASGRO handles different specimen geometries, the crack growth in Kb and C(T) specimens were simulated in NASGRO. The same material file was used for both specimen types. This material file was obtained from fatigue crack growth testing using Kb specimens. The Kb specimen was modelled as a SC01 model in NASGRO while the SS02 model was used for the C(T) specimen. The models were given dimensions corresponding to the specimens used for mechanical testing at GKN. In Figure 4.3 it can be seen that NASGRO predicts the Kb specimen (blue line) to have the same propagation rate as the C(T) specimen (yellow dashed line). This tells us that the NASGRO software as it is used at GKN is not able to handle any differences in crack growth rate related to specimen geometry.

The NASGRO program has the possibility to handle the influence of load history in four different ways, Constant closure, Generalized Willenborg, Chang-Willenborg and Strip yield. With the strip yield option, NASGRO calculates an opening stress intensity factor K_{op} based on the plasticity induced stresses at the crack tip, i.e. it simulates plasticity induced crack closure. When the investigation above was done with the strip yield option, NASGRO showed a difference in predicted crack growth rate between Kb and C(T) specimens, as seen in Figure 4.3. As indicated in the figure, cracks in Kb specimens are predicted to grow faster than cracks in C(T) specimens by a factor of 1.42, for a $^{\Delta K}/_{K_{Ic}}$ value of 0.25.

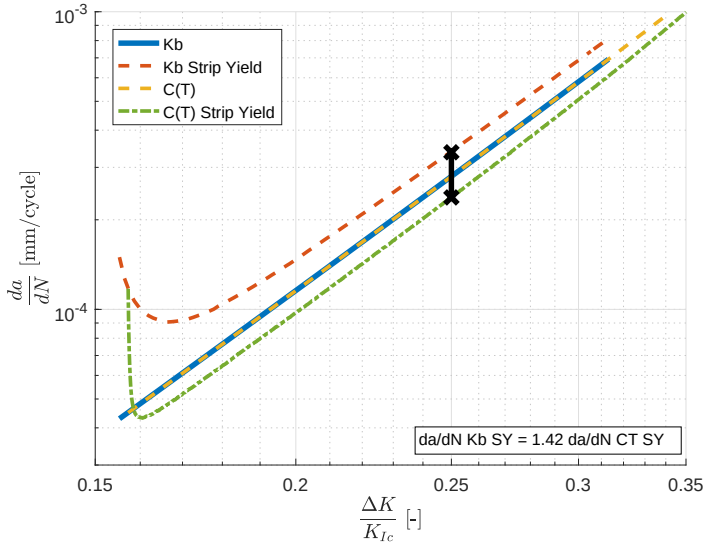

Figure 4.3: *Predicted fatigue crack growth rates for Kb and C(T) specimens*

4.4 Evaluation of plastic zone size using FEM

In order to investigate the size of the plastic zone and the stress state at the crack tip, and to evaluate whether there are differences between the specimen types which could explain the difference in FCGR, a finite element analysis was performed. Here the modeled specimens were loaded in static tension to evaluate a monotonic plastic zone. The simulations were performed within the ANSYS Workbench 19.0 suite. The geometries of the specimens were modelled in Ansys DesignModeler which is integrated in Ansys Workbench. Since both specimens have double-folded symmetries one quarter of each specimen was modelled, cf. Figure 4.4. The dimensions of the models were based on the specimen drawings in Figure 2.2 and 2.3. For the Kb specimen only the rectangular part of the specimen was modelled. In order to be able to use the models later for specimens with other dimensions and to easily be able to adjust the crack lengths the models were parameterized for more or less all dimensions.

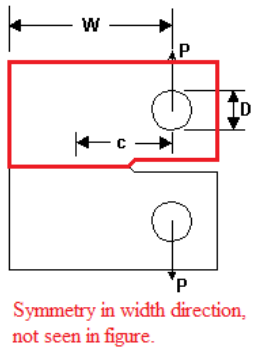

(a) *C(T) specimen symmetry.*

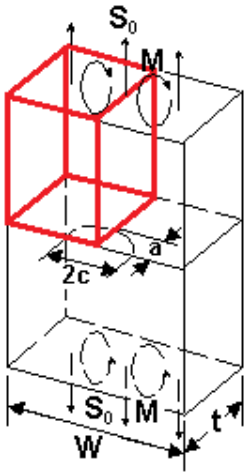

(b) *Kb specimen symmetry.*

Figure 4.4: *Symmetry of specimens. Areas marked in red were modeled in Ansys.*

4.4.1 Mesh

In order to capture the plastic zone size, the volume around the crack tip has to be resolved with small and structured elements. To achieve this, the crack front has been placed on one side of a cuboid, called the core, that goes through the width of the specimen. The cuboid has then been enclosed in two half circles which have been sweept around the core, in the same manner as described by Roychowdhury and Dodds [22]. The core enclosed in the inner half circle can been seen in Figure 4.5. Note that both the core and circles have been curved for the Kb specimen to be able to follow the crack front which has been assumed to have the shape of a half circle, i.e $a/c = 1$. The size and shape of the elements in the core have been controlled by a face sizing command at the end surfaces of the core (located at the free and symmetry surfaces). Rembeck and Sjöblom [16] found that the plastic zones have to contain at least 5–10 elements, therefore the size of the elements in the core have been found by an iterative process. A mesh was created and the model solved. This was then repeated until the plastic zone contained at least 10 elements. In Table 4.3 the size of the three features are presented along with the element size of the elements in the core for each specimen type. Here, L_{core} denotes the length of the quadratic sides of the core cuboid, L_e denotes the edge size of the elements in the core while R_{inner} and R_{outer} denote the radius of the circles enclosing the core.

Table 4.3: *Dimensions of features near the crack front.*

	L_{core}	L_e	R_{inner}	R_{outer}
C(T)	0.12 mm	0.005 mm	$4L_{\text{core}}$	$3R_{\text{inner}}$
Kb	0.3 mm	0.0075 mm	$3L_{\text{core}}$	$2R_{\text{inner}}$

The stress gradients in the specimens are expected to be sharper near the surface of the specimen compared to the mid-plane, therefore the in depth-size of the elements near the surface has been set smaller than for the elements at the symmetry plane, cf. Roychowdhury and Dodds [22]. This was done by an Edge Sizing Biasing factor, where the crack front and all aligned edges were divided by 25 elements with a bias factor of 20 for the C(T) specimen and 10 for the Kb specimen.

For the Kb specimen it was not possible to get a perfectly structured mesh. The problem was to address two sweeping methods for the two half circles, one around the core and another from the free surface to the symmetry plane. It was not possible to do this, so only the sweeping around the core was performed, which led to element shape distortions from the crack front and into the traction free part of the crack. This can bee seen in Figure 4.7a. Since this part of the model is unconstrained and the load level is low, the impact of the distortion was judged to be low.

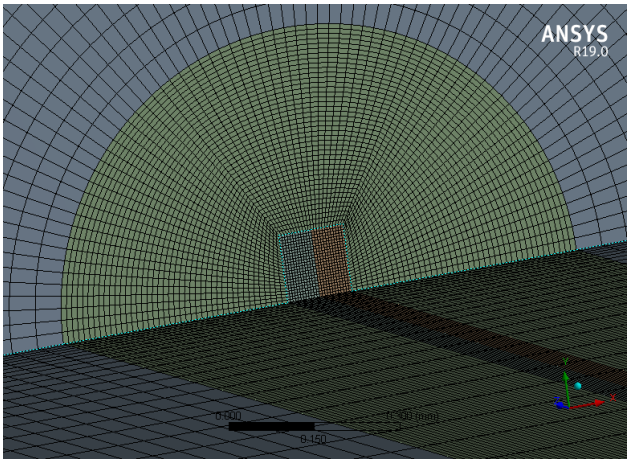

(a) *C(T) core mesh*

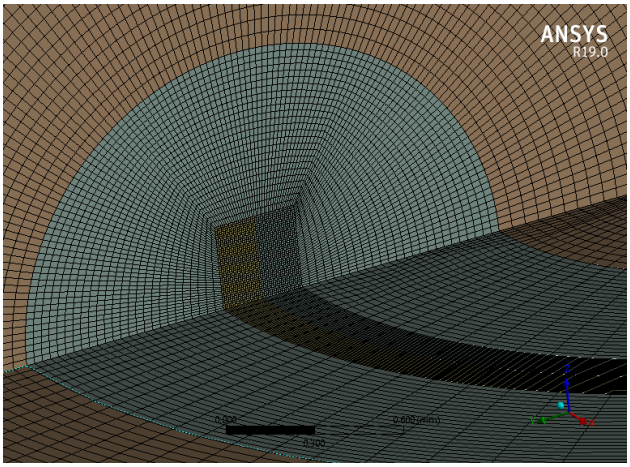

(b) *Kb core mesh*

Figure 4.5: *Mesh of the core and the inner half circle*

4.4.2 Boundary conditions

In order to compare results from the C(T) and Kb simulations, the crack in each simulation has to have the same load level, i.e ΔK. Based on the results of the discrepancies quantification, $\Delta K = 20\,\mathrm{MPa}\sqrt{\mathrm{m}}$ was chosen as a relevant load level. From this, one has to define a stress and crack size combination which gives the desired value. Here two slighty different approaches were used for the C(T) and Kb specimen. For the Kb specimens used at GKN the crack size ranges from approximately 0.5 to 3 mm during a FCGR test, however, since the physical size of the Kb specimen is smaller compared to the crack size than for a C(T) specimen, it was not possible to place the crack freely in that range and still be able to fit the structured mesh. Instead a crack size of 2 mm was chosen since that is close to the center of the specimen. From there, a nominal stress load was calculated using the SC01 geometry in NASGRO. For the C(T) specimen the procedure was the opposite. First a load level was chosen based on the test reports from FCGR testing and then a crack length was calculated using the SS02 model in NASGRO. Nominal load levels and crack sizes can be seen in Table 4.4. Note that for the C(T) specimen the applied simulation load is half the load in the table due to symmetry. For the C(T) specimen the load was applied as a force at the upper half of the hole in the specimen, indicated by label A in Figure 4.6a. The load on the Kb specimen was applied as stress on the top surface of the specimen, indicated by label A in Figure 4.6b. The load was applied as a pulsating tension- load, i.e. $R = 0$

Table 4.4: *Applied nominal load, crack size and stress intensity factors*

	Nominal load	**Crack size**	ΔK	R
CT	1166 N	20.2 mm	$20\,\mathrm{MPa}\sqrt{\mathrm{m}}$	0
Kb	361 MPa	2 mm	$20\,\mathrm{MPa}\sqrt{\mathrm{m}}$	0

Each specimen has two symmetry surfaces which where constrained by a displacement that forces the constrained surface to only move in the in-plane direction, i.e the out of plane displacement was set to zero. The symmetry surfaces of the C(T) specimen are shown in Figure 4.6a and indicated by label B and C, while the corresponding surfaces for the Kb specimen are shown in Figure 4.6b and indicated by label C and D. To prevent rigid body motions the model has to be constrained in all directions. Since the specimen only are constrained in two direction by the symmetry condition both specimens are able to move in one direction. For the C(T) specimen this was arranged by a zero displacement constraint applied to the back end edge, shown in Figure 4.6a by label D. The Kb specimen was fixed in space by a fixed support on one corner of the specimen, indicated in Figure 4.6b by label B.

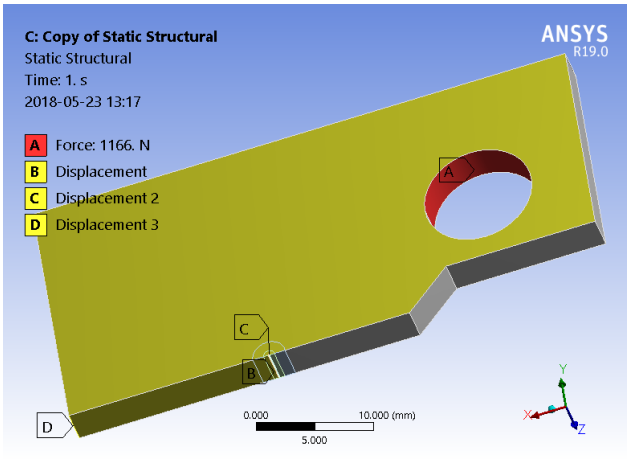

(a) *C(T) specimen.*

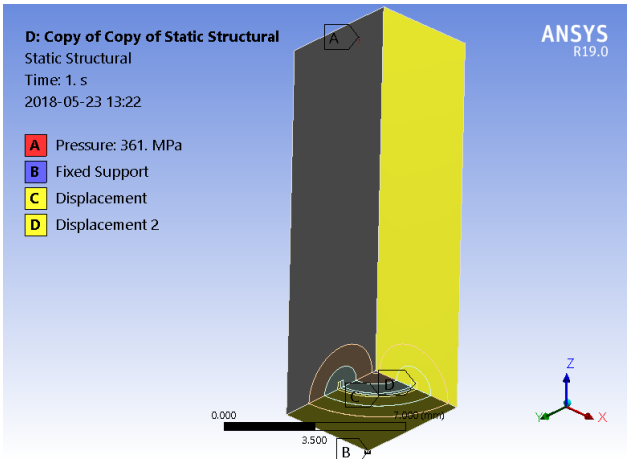

(b) *Kb specimen*

Figure 4.6: *Areas where loads and boundary conditions are applied*

4.4.3 Constraint level at the crack front

Several authors, such as [2, 9, 11], have proposed that the T-stress might not be negligible and in some cases this can be used to explain differences in FCGR seen between different specimen geometries. To investigate if the T-stress in C(T) and Kb specimens are non zero, and if so, if they are different between the specimen types, a so called fracture analysis in Ansys was incorporated into the FEM simulation. The crack was defined as a "Pre-Meshed Crack" by a selection of the nodes on the crack front. The default value of 6 solution contours was used, meaning that the fracture results are calculated in 6 contours around the crack tip. Two fracture results were selected, namely T-stress and the Mode I stress intensity factor. The stress intensity was included to verify that the correct load and crack length combinations to achieve $\Delta K = 20\,\mathrm{MPa}\sqrt{\mathrm{m}}$ were used and to evaluate how the stress intensity varied along the crack front.

4.4.4 Analysis settings and model statistics

For both models linear elements were used, the C(T) model consisted of 230 850 elements while the Kb model consisted of 198 590 elements. Since a non linear material model is used, the solver has to be non linear as well. Here a full Newton-Raphson iteration solver was used. To help the solver to converge, the load was applied in ten uniformly divided load steps.

4.4.5 Material model

To be able to capture the plastic behavior of the material, a non-linear material model must be used. Here a multilinear material model with isotropic hardening has been used. The material is defined by Young's modulus and Poisson's ratio for the linear elastic response, while 19 stress-strain points define the non-linear behavior beyond yielding. The non-linear strain is given as plastic strain ε_p, where GKN defines $\varepsilon_\mathrm{p} = 0$ as the strain which gives 0.03% permanent strain when unloading. The material is cast Ti-64 and the material properties have been evaluated by GKN and are the same as used in in-house simulations.

Plastic zone

To be able to calculate the size of the plastic zone one has to define what the plastic zone implies. In this work the plastic zone has been defined as those nodes that have a von Mises equivalent stress equal to or greater than the yield stress. The yield stress is defined as the stress which gives 0.2% permanent strain after unloading. The core, which is dived to 25 elements, is enclosing the plastic zone. Since the core is divide into 25 elements there are 26 planes with nodes along the crack front where the size of the plastic zone can be evaluated. At each plane the distance from the crack front to the plastically deformed nodes has been calculated, and the size of the plastic zone has been defined as the greatest distance. This is illustrated in Figure 4.7b where each blue circle represents a plastically deformed node and the the red line illustrates the size of the plastic zone.

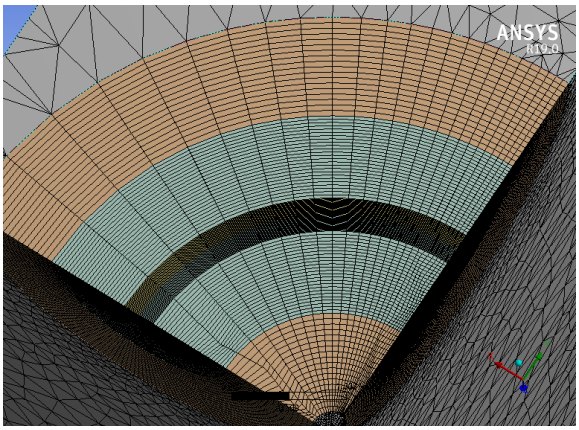

(a) *Distortion in the mesh of the Kb-specimen*

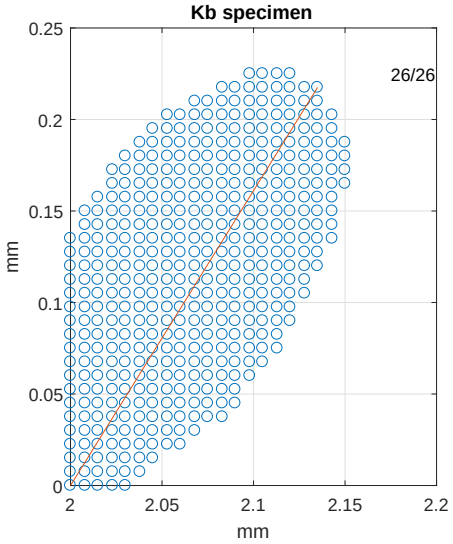

(b) *Definition of the plastic zone size. Each blue circle represents a plasticly deformed node. The red line indicates the largest distance from the crack front to a plastic node*

Figure 4.7

4.4.6 Results

The results from the plastic zone size analysis is presented in Figure 4.8, where the results in Figure 4.8a are calculated as described in section 4.4.5. One can see that the plastic zone size is greater for the Kb specimen than for the C(T) specimen. As a reference, the plastic zone size according to the Irwin approximation, cf. equation 3.3, are shown. It is seen that the the results from the C(T) specimen is within the reference interval. For the Kb specimen, the result is within the theoretical interval for approximately 85% of the crack front. A possible reason why the plastic zone for the Kb specimen is greater than the plane stress condition estimation can be that the reference line in Figure 4.8a is calculated for one ΔK value, but NASGRO and the stress intensity results in this simulation (cf. Figure 4.9a) predicts that the stress intensity factor varies along the crack front and are greater near the free surface of a specimen than in the center where the symmetry plane is located.

When studying the shape of the plastic zone by the type of plot shown in Figure 4.7b concerns were raised that the area of the plastic zone in the C(T) specimen should be greater near the surface than at the center of the specimen, and that this tendency was not captured by the used definition of the plastic zone. Therefore the area of the plastic zone size was calculated by multiplying the number of plastic nodes by the cross sectional area of one element in the core, i.e L_e^2. The results from this investigation are shown in Figure 4.8b and it is seen that that the area of the plastic zone is now increasing near the surface. This behavior was not captured by the plastic zone size estimation shown in Figure 4.8a. On the other hand the objective of this simulation was to compare the plastic zone size in the Kb specimen with that of the C(T) specimen. For this purpose the results are in line and shows that the plastic zone is greater in a Kb specimen than in a C(T) specimen.

In figure 4.9 the results from the fracture analysis are shown, with the stress intensity factor along the crack front shown in Figure 4.9a. The intention was to load the crack with $\Delta K = 20\,\mathrm{MPa}\sqrt{\mathrm{m}}$. The results are reasonable close to that. It is seen that the stress intensity factor, SIF, varies along the crack front for both the C(T) and Kb specimen. The SIF for the C(T) specimen is greater at the symmetry plane than near the free surface and vice versa for the Kb specimen. The nominal stress intensity is indicated in the figure as a reference. For the Kb specimen, the SIF at the c-tip of the crack is indicated as well since NASGRO predicts the stress intensity to be different at the c-tip as compared to at the a-tip. T-stress normalized by the yield stress is presented in Figure 4.9b. The T-stress is clearly non-zero for all of the test specimens. For the C(T) specimen, the T-stress is positive and almost constant along the crack front, while for the Kb specimen the

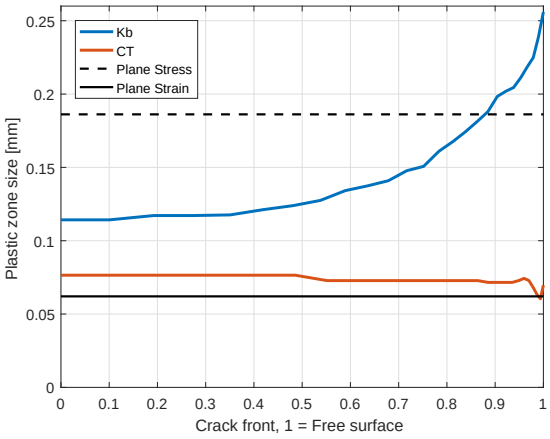

(a) *Plastic zone size along the crack front for Kb and C(T) specimens, compared to the Irwin approximation in [2]*

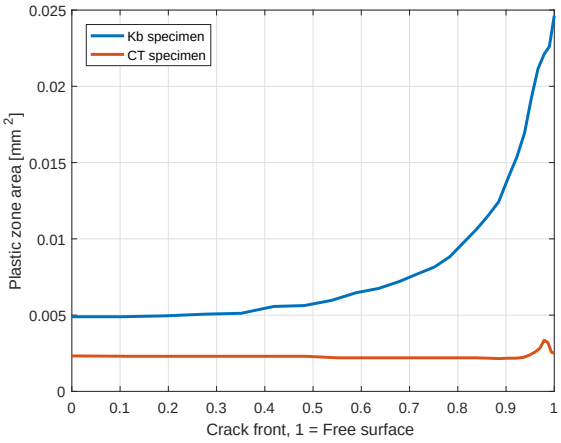

(b) *Approximation of the area of the plastic zone.*

Figure 4.8: *Plastic zone size*

T-stress is negative and varying more along the crack front. Near the free surface results are fluctuating very much which probably is due to difficulties in resolving the stress gradients near the surface.

For a discussion of how the results relate to the fatigue crack growth rate, the reader is referred to section 5.

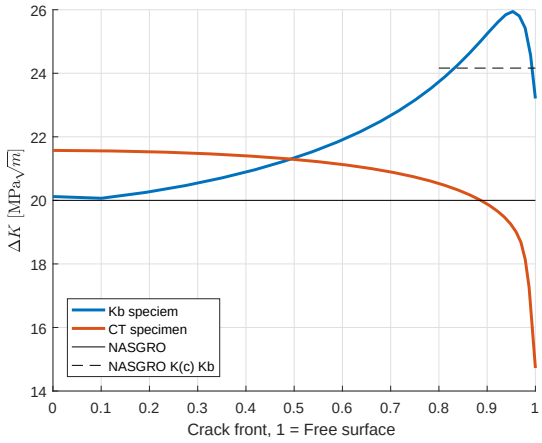

(a) *Stress intensity factor along normalized crack front compared to the NASGRO results for the same crack size and load level.*

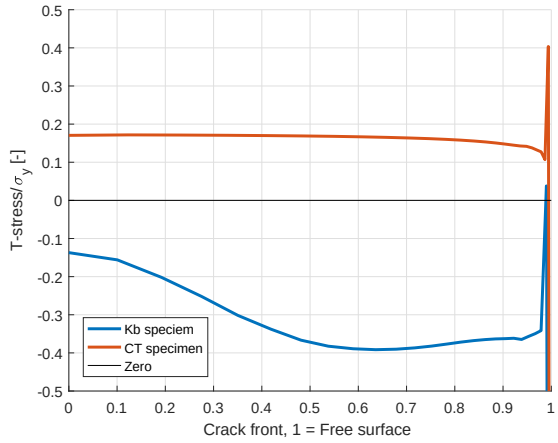

(b) *T-stress normalized by yield stress along normalized crack front*

Figure 4.9: *Fracture mechanics results along the crack front.*

4.5 Fatigue crack growth rate test in forged C(T) specimens

Since only cast material at GKN has been tested using both Kb and C(T) specimens, it is hard to know if the discrepancies found are only affected by the difference in specimen geometry or if the cast material has some properties that give rise to this great difference in crack growth rates.

Forman and Mettu [19] conclude that FCG rates for standard specimens, C(T) and SEB, can be used with "reasonable accuracy" for surface flaw specimens, i.e Kb-specimens. In their study Ti-64 bars were used for specimen manufacturing. To verify Forman and Mettus conclusion and to investigate if their conclusion holds for forgings as well, crack propagation tests using C(T) specimens were performed for forged Ti-64 and IN-718. The forged materials were assumed to have similar properties as their Ti-64 bar material.

4.5.1 Test material and specimens

GKN have FCGR data for forged Ti-64 and IN-718. Both are generated from testing using Kb specimens. Spare material from the Kb-testing was used for the C(T)-testing, this minimizes the risk of material manufacturing effects affecting the results. One of the objectives with the testing was to compare differences in FCGR rate between cast and forged materials. The specimen used was a C(T) specimen according to Figure 2.3 with a thickness of $B = W/6$. This is the same specimen type and size that GKN used for testing of cast C(T) specimens.

4.5.2 Test conditions

As discussed above, the discrepancies between C(T) and Kb specimens occur at all temperatures, R-ratios and for all investigated cast materials. Due to this, the testing of C(T) specimens in forgings was restricted to the material Ti-64 and IN-718 at room temperature and stress ratio $R = 0.05$. The stress ratio for C(T) specimens has to be greater than zero due to the gripping method employed. One specimen of each material was tested. The specimen preparation and testing was performed at Metcut Research Inc. in USA and performed according to Table 4.5

Table 4.5: *Test environment and parameters*

Test method	Measurement of fatigue crack growth rates
Test standard	ASTM-E647
Specimen type	C(T)
Waveform	Triangular for Paris region Sinusoidal for pre-cracking
Frequency	10 Hz for Paris region 30 Hz for pre-cracking
R	0.05

4.5.3 Results

Results from the testing are presented in Figure 4.10 , along with data previously generated from Kb specimens. The data is presented as described in section 4.1. It is seen that the there is a difference between the specimen types where cracks in a Kb specimens are growing faster than the cracks in C(T) specimens. However, the difference is much less pronounced than for cast materials. The cracks in Kb specimens are growing about 20% faster than the crack in the C(T) specimen for Ti-64 forging and 30% faster for IN-718. As in section 4.1, the predicted life, P, of the specimen calculated in NASGRO using a Kb specimen based material model were compared to the actual life, A. The A/P result are compiled in Table 4.6, where it is seen that the A/P value is greater for the C(T) specimens than for the Kb specimens, meaning that a crack is estimated to grow faster in a Kb specimen than in a C(T) specimen. For cast materials the differences were much more pronounced, see section 4.1.2.

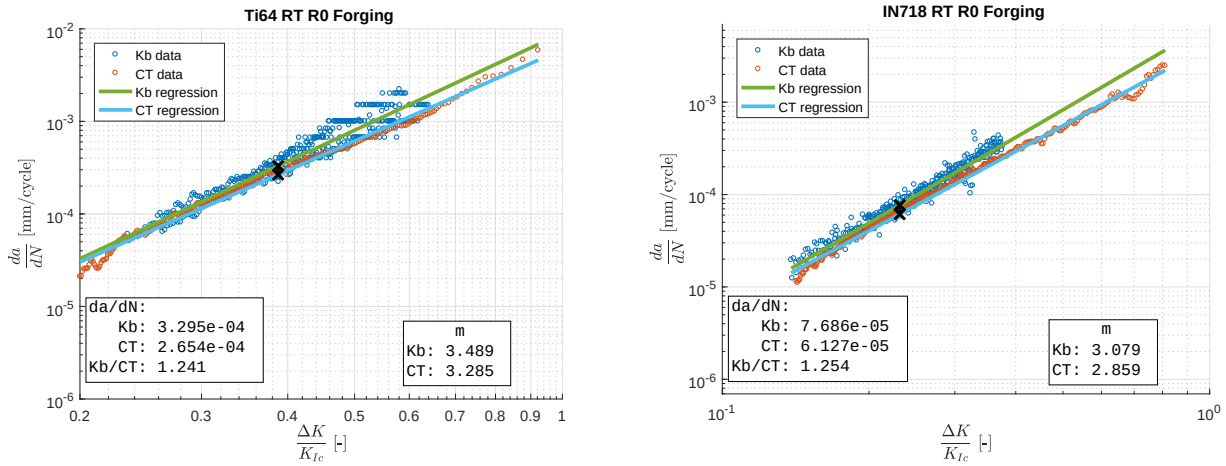

(a) *Ti-64* **(b)** *IN-718*

Figure 4.10: *Fatigue crack growth in forged material*

Table 4.6: *Actual over predicted life, A/P, for forged Ti-64 and IN-718 using crack growth parameter values fitted to Kb specimen data.*

Specimen	CT1	Kb1	Kb2	Kb3	Kb4
Ti-64	0.82	0.64	0.70	0.66	
IN-718	0.99	0.67	0.73	0.61	0.72

4.6 Grain size

Castings are known to have large grains. To investigate reasons for differences in crack growth rates between Kb and C(T) specimens it would be interesting to compare the grain size to the size of the crack and the plastic zone. In order get that information, grain sizes of a couple of used FCGR specimens were measured. Grain size measurements were performed by authorized lab personal from the material laboratory at GKN.

4.6.1 Sample preparation

Samples made out of Ti-64 and IN718 were prepared[1]. The creation of material samples includes a number of steps. First of all the material must be be cut up into smaller dimensions to fit into the microscope, secondly the surface on which the grain size is measured has to be processed to make the grains visible. This is done by grinding the surface with finer and finer grinding papers. Then the sample surface is polished and finally etched.

When the surface preparation was done, a microscope with the capability to take pictures was used to photograph the entire surface. The microscope can only cover a part of the sample at once so a picture of the entire sample was built up by several smaller individual pictures. The software used with the microscope (NIS-Elements) has the ability to automatically make a composed picture of the sample surface.

The grain size in a microstructure is presented in the form of a ASTM-number, G, [23], which correlates to an average grain diameter, $\bar{d}$ and an average cross sectional area of the grain, $\bar{A}$. The normal procedure to determine G is to calculate the number of times a line crosses a grain boundary. However, to use this method the line has to be crossed by at least 50 grain boundaries. The grains in the samples prepared for this work were so large that it was not possible to fit 50 grains onto one sample. The work around to this problem were to use the ALA (As Large As) method instead, cf. [24]. When using the ALA method, one has to determine

[1]The microstructures in Ti-64 and Ti-6242 were assumed to be similar enough to only measure grains in one of the materials.

the average cross sectional grain area, $\bar{A}$, and then find the ASTM-no. from a table or by equation (4.2)

$$G = 3.321928 \cdot \log\left(\frac{1}{\bar{A}}\right) - 2.954 \tag{4.2}$$

To calculate the average grain area NIS-Elements was used. In NIS-Elements it is possible to freely mark a part of the picture. The software then calculates the area of that part. The procedure can be repeated and the software provides the average area of the marked parts. To calculate the average area, only the samples made from C(T) specimens were used since the grains were so big that the Kb samples contained very few grains that were fully enclosed within the sample. In Figure 4.12 and 4.13 the measured grains in Ti-64 and IN-718, respectively, can be seen along with the area of each grain.

4.6.2 Results

In Table 4.7 the measured average grain size and the corresponding ASTM-number are presented, as well as an estimated average grain diameter. In Table 4 in ASTM E112 [23] the average grain diameter for ASTM-numbers are presented, but the grains in the samples used here were greater than those include in ASTM E112. Instead the average diameter, d, was evaluate based on the assumption of perfectly round grains

$$d = 2\sqrt{\frac{\bar{A}}{\pi}} \tag{4.3}$$

The same microstructual properties for the IN-718 forging used for fatigue crack growth rate testing using C(T) specimen are also presented. These microstructure properties were retrieved from [25]. For forged Ti-64 where no measured grain size could be found, a photograph of the microstructure presented in Figure 4.11, [26] is used instead. The average grain diameter in cast Ti-64 was estimate as 2.4 mm whilst the estimate grain diameter for cast IN-718 was 1.9 mm. The measured grain size in cast Ti-64 is in line with the results of Sen et al. [20], who found the grain size to be 1.7mm. The grain sizes in cast materials are approximately 100 times the size of the grain in the forged material. Since the estimated mean grain diameter is based on a cross section of the specimen, the estimated value should be lower than the actual grain size. In Figure 4.12 and 4.13 the microstructure can be seen. The grains in Ti-64 appear to be more symmetrical than those in IN-718. Photographies of all prepared samples can be seen in Appendix B.

Table 4.7: *Microstructure properties in Ti-64 and IN-718*

	Cast			Forging		
Material	**Avg. area**	**ASTM-no.**	d	**Avg. area**	**ASTM-no.**	$\bar{d}$
Ti-64	$4.4\,\text{mm}^2$	-5	2.4 mm	See Figure 4.11		
IN-718	$2.8\,\text{mm}^2$	-4.5	1.9 mm	$504\,\mu\text{m}^2$	8.0	0.0224 mm

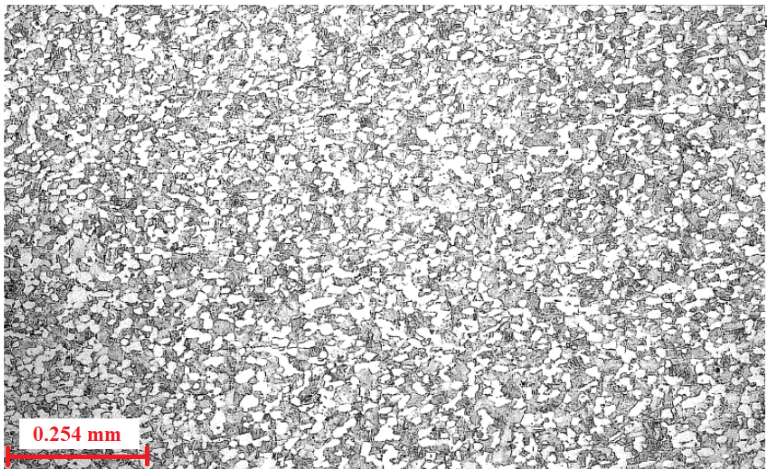

Figure 4.11: *Microstructure of forged Ti-64, [26].*

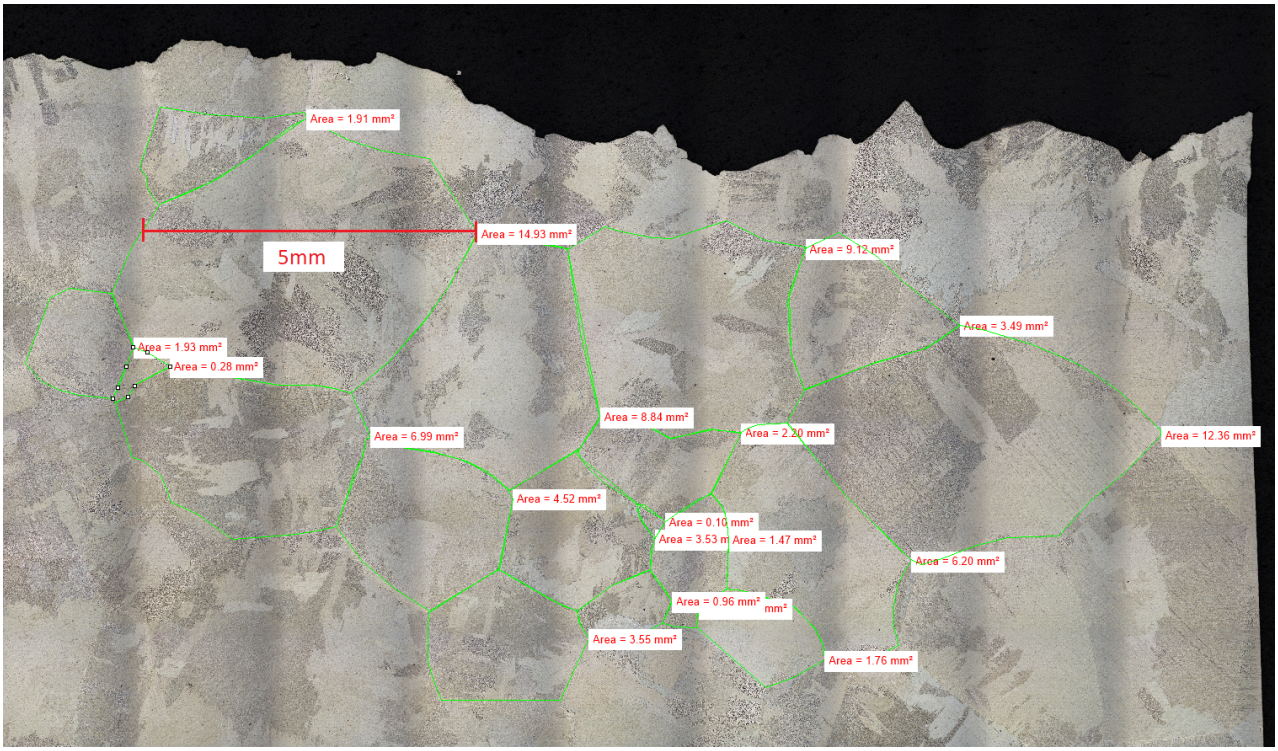

Figure 4.12: *Measuring of grain area in cast Ti-64*

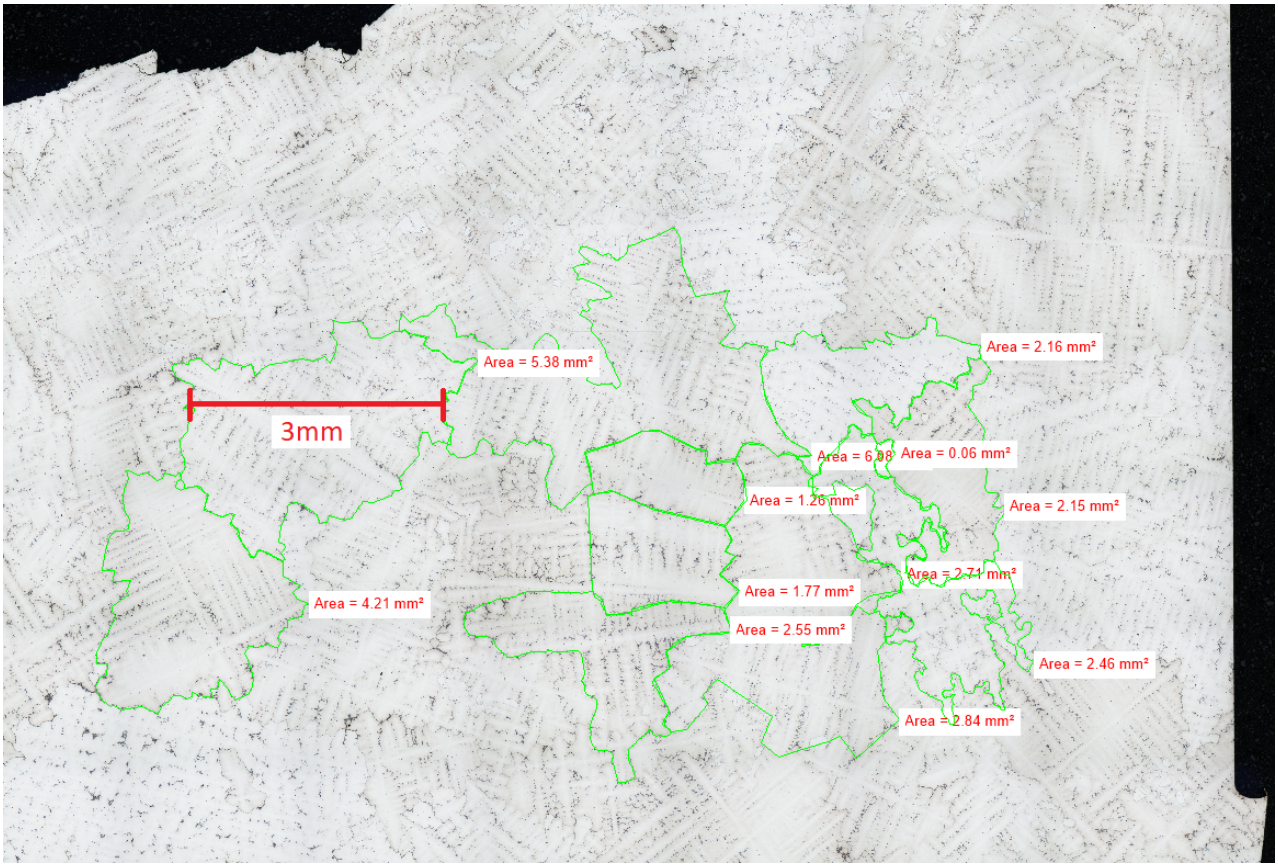

Figure 4.13: *Measuring of grain area in cast IN-718*

5 Discussion

As seen in section 4.1 there is a distinct difference in fatigue crack growth rates in Kb specimens compared to C(T) specimens for castings. In Table 4.2 the difference is quantified and the cracks in the Kb specimens are found to consistently grow faster than cracks in C(T) specimens. Since this difference is observed for three different materials, two different stress ratios and for temperatures ranging from room temperature to 650°C it can not be neglected, nor explained by scatter in test results. Neither is it likely that such a clear difference can be explained by incorrect test methods since the ASTM standard, [6, 27], for fatigue crack growth testing has been applied. When evaluating fatigue crack growth in Kb specimen, the crack length is determined by optical measurements of the crack length at pre-crack and final crack and from PD records. Since the fracture surfaces in castings are very rough it can be difficult to measure the pre- and final crack lengths. There have been concerns at GKN that poorly measured crack lengths may have a severe influence on the evaluated fatigue crack growth rates. From the results in section 4.2 it can bee seen that the measure of crack lengths in Kb specimens can effect the fatigue crack growth, but in relation to the difference in fatigue crack growth rates between Kb and C(T) specimen the influence of measured crack lengths is small. It is also unlikely that the optically measured crack lengths in Kb specimen should be consistently wrong, and thereby explain the observed difference in fatigue crack growth between Kb and C(T) specimens.

In section 4.5 measured fatigue crack growth rates in forgings using both Kb and C(T) specimens are presented. It is seen that there is a small difference in fatigue crack growth rates with cracks in Kb specimens growing slightly faster than cracks in C(T) specimens. The difference in fatigue crack growth rates in Kb specimens compared to C(T) specimens is much less pronounced for forgings than for castings. For forgings the difference is approximately 25% whilst for castings loaded with $R = 0$ the fatigue crack growth rates are on average 360% faster in Kb specimens as compared to C(T) specimens. The fatigue crack growth rate results in forgings for C(T) specimens are based on one specimen for Ti-64 and one specimen for IN-718. Two specimens are probably not enough to be able to make formal conclusions, but they provide a good indication of the behavior.

C(T) specimens are the most used test specimen type, meaning that the test laboratory have good knowledge of fatigue crack growth testing using C(T) specimens. Furthermore, GKN's experience is that forgings are easiest to obtain reliable test results from. If we compare the fatigue crack growth results from testing in forgings with data from Forman and Mettu [19] who performed fatigue crack growth testing in bars of Ti-64, cf. Figure 5.1, we can see that the fatigue crack growth rates are similar in forgings and bars. This also strengthens the conclusions from fatigue crack growth testing in forgings using C(T) specimens since bars and forging are assumed to have similar crack growth characteristics.

The results in section 4.3 show that NASGRO predicts faster crack growth rates for Kb specimens than for C(T) specimens if the strip yield model for handling load history is used. The results from the NASGRO investigation were used as a motivation to conduct a more formal plasticity simulation using the finite element method. This study is presented in section 4.4. When starting the finite element analysis the idea was that a large plastic zone should give more residual stresses at unloading and thereby give more plasticity induced crack closure that slows the fatigue crack growth. With this reasoning and the fact that the results from the fatigue crack growth test in forgings using C(T) specimens at this time were unknown, the C(T) specimen were expected to have a larger plastic zone. The results from the FEM analysis in Figure 4.8 is however opposite to the expected outcome, the plastic zone was found to be greater for the Kb specimen than for the C(T) specimen.

Since GKN have had the fatigue crack growth test results in castings for approximately 10 years they have during that time assumed that the geometry of test specimens can have a large influence on the test results. This assumption was the starting point for this thesis project. When the test results from the fatigue crack growth testing in forgings using C(T) specimens were delivered from the test laboratory this assumption had to be modified. The observed difference in fatigue crack growth rates between Kb and C(T) specimens in castings is still distinct, but it can not solely be explained by the difference in geometry of the test specimens, since the difference for forgings was minor. Consequently, there must to be something in the cast materials that triggers

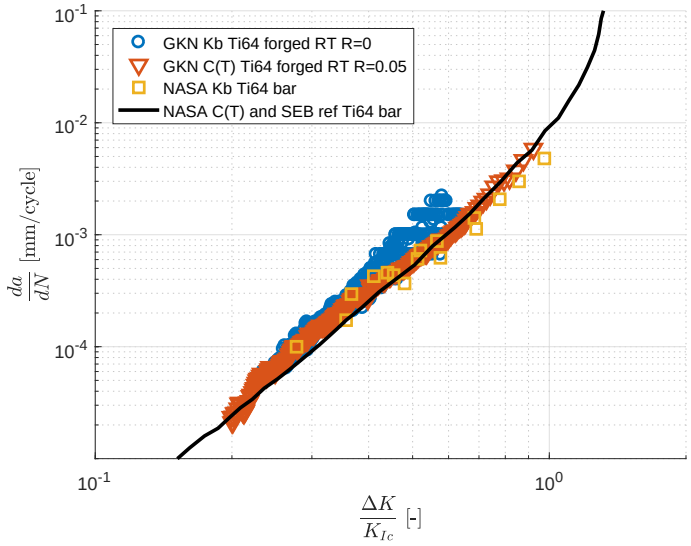

Figure 5.1: *Fatigue crack growth test results for forged Ti-64 and bars of Ti-64, [19]*

this difference in fatigue crack growth rates.

In the literature discrepancies in fatigue crack growth rates between specimen geometries have been reported. It is common that the near threshold region has been studied, e.g. [12]. Suresh [2] reports that for low ΔK where the plastic zone is smaller than the grain size, a crystallographic fracture process is promoted, which results in a serrated fracture surface. The rough fracture surface is leading to surface roughness induced crack closure. When comparing the results from the plastic zone size analysis in Figure 4.8a with the measured grain sizes in casts in Table 4.7 it is clear that the the plastic zone is smaller than the grain size. From this comparison one could argue that the fatigue crack growth specimens made of cast material can be affected by roughness induced crack closure in the entire Paris region. Walker et al. [28] investigated the crack propagation and crack closure in β-annealed Ti-64 using ESE(T)[1] specimens. The β-annealed Ti-64 is reported to have a coarse grain structure with a grain size of 1.2 mm. Walker et al. found ESE(T) specimens with the same width and thickness as the C(T) specimen in this study to have a closure function $f = \frac{P_{\text{op}}}{P_{\text{max}}}$ ranging from approximately 0.7 to 0.25 for crack length to width ratios, $^{c}/_{W}$, ranging from 0.5 to 0.8. The research by Walker et al. supports the theory of surface roughness induced crack closure in specimens made from cast material.

If the theory of surface induced crack closure affecting the cracks in specimens made from castings is correct it is still to be explained why cracks in C(T) specimen are influenced more of roughness induced crack closure than cracks in Kb specimens. Two possible hypothesis to this difference is: i) The fracture surface is larger in C(T) specimens than in Kb specimens, and these larger fracture surfaces promotes more asperities to match at unloading. ii) The load in a Kb specimen is well distributed over the the cross section of the specimens which should keep the fracture surface more or less parallel during loading and unloading. For the C(T) specimens one can image the upper and lower half of the specimens to behave as a beam loaded with a point load at one edge and clamped at the other end. This could result in the fracture surfaces being separating through a bending motion that would not keep the the fracture surfaces parallel.

To fully understand why cracks in Kb specimens are growing faster than cracks in C(T) specimens when the specimens is made of cast material, more research has to be done. It would be interesting to perform crack propagation testing using both Kb and C(T) specimens and record the opening stress intensity factor, K_{op}, to investigate if cracks in C(T) specimens are subjected to more crack closure than cracks in Kb specimens. The opening stress intensity factor can be found by recording the back-face strain compliance as done by Walker et al. [28] or from the PD-method as done by Andersson [29].

[1] Eccentrically Loaded Single Edge-Notched Tension. Have the same geometry and notch as C(T) specimen, but with a greater height.

The theory of linear elastic fracture mechanics, LEFM, is based on the assumption of a homogeneous and isotropic material. For forgings this assumptions is reasonably correct since the grain size is far smaller than the plastic zone and the dimensions of the cracks. The fatigue crack growth test results in forgings using C(T) and Kb specimens validates that the use LEFM is applicable for forgings since both specimen types gives the same propagation rate. For castings on the other hand one could question if the assumption of a homogeneous and isotropic material is applicable. The casts in this study featured grain sizes clearly greater than the plastic zone size and the crack lengths in Kb specimens are one same order as the grain size, in fact even grains double the size of the cracks in Kb specimens have been observed, cf Figure 4.12 and Appendix B. If LEFM is not applicable for cast materials and the studied geometry of test specimens, the problem is that there are no other generally accepted tools for predicting crack growth. This implies that one is forced to produce geometry dependent material properties. Furthermore, the inhomogeneity would result in large scatter between test, which also is seen in Figure 4.1 and Appendix A of this study.

6 Conclusions

Fatigue crack growth in titanium and nickel based alloys has been studied. The main objective has been to study how the geometry of the test specimen influences the fatigue crack growth rate. To this end, the plastic zone size has been evaluated through a numerical simulation, the grain sizes in castings have been measured, and the influence of measured pre-crack and final crack lengths on the estimated crack growth rates has been investigated. Based on these investigations the following can be concluded:

- For Kb and C(T) specimens made from *castings* it is concluded that cracks are growing faster in Kb specimens than in C(T) specimens. For specimens loaded with $R = 0$, cracks are growing roughly 3.6 times faster in Kb specimens than in C(T) specimens.
- Possible incorrectly optically measured pre-crack and final crack lengths have been found, but are shown to not solely explain observed difference in fatigue crack growth rates between Kb and C(T) specimens made from castings.
- For Kb and C(T) specimens made from *forgings* the difference in fatigue crack growth is admissible and on the order of 20%.
- The grain size in cast Ti-64 and IN-718 is on the order of 100 times as large as grains in forged Ti-64 and IN-718 (2 mm versus 0.02 mm).
- It is likely that the greater fracture surfaces of C(T) specimens compared to Kb specimens permits more surfaces roughness induced crack closure, giving a slower crack growth rate in C(T) specimens than in Kb specimens.

6.1 Future work

The mechanisms causing cracks in Kb specimens made from castings to grow faster than cracks in C(T) specimens is not fully understood. The dimensions of the microstructural features is likely to be a main cause of the variations in fatigue crack growth rates, possibly due to altered roughness induced crack closure. The influence of crack closure is proposed to be studied by recording closure levels during fatigue crack growth test of Kb and C(T) specimens made from castings.

The size and characteristics of the plastic zone in Kb and C(T) specimens is proposed to be further examined. Finite element analysis results from this study show that the monotonic plastic zone size in Kb specimens is approximately two times as large as the plastic zone in C(T) specimens when both specimens contain a crack with a stress intensity factor of $20\,\mathrm{MPa}\sqrt{\mathrm{m}}$. This is puzzling since C(T) specimens are more likely to be subjected to plane stress than Kb specimens and the plastic zone should therefore according to equation (3.3) be greater in the C(T) specimen than in the Kb specimen. Further, the cyclic plastic zone should be evaluated since it is more relevant for fatigue crack growth.

References

[1] T.L. Anderson, *Fracture Mechanics, Fundamentals and Applications*, 2nd ed. Boca Raton FL: CRC Press, 1995.

[2] S. Suresh, *Fatigue of Materials*. Cambridge: Press Syndicate of the University of Cambridge, 1992.

[3] N. E. Dowling, *Mechanical Behavior of Materials, Engineering Methods for Deformation, Fracture, and Fatigue*, 4th ed. Essex England: Pearson, 2013.

[4] H. Tada, P. C. Paris, and G. R. Irwin, *The Stress Analysis of Cracks Handbook*, 3rd ed. New York NY: Professional Engineering Publishing, 2000.

[5] NASGRO, *Fracture mechanics and fatigue crack growth analysis software, Reference manual*, version 6.21 Final, Jan. 2012.

[6] ASTM E647-15e1, *Standard Test Method for Measurement of Fatigue Crack Growth Rates*. ASTM International, 2015.

[7] N. Axelsson and J. Baric, "Improved data regression methods for crack growth characterization", M.S. thesis, Applied Mechanics, Chalmers University of Technology, Gothenburg, Sweden, 2016.

[8] D. C. Lay, *Linear Algebra and Its Applications*, 4th ed. Boston MA: Pearson, 2012.

[9] P. Hutař, S. Seitl, and Z. Knésl, ''Quantification of the effect of specimen geometry on the fatigue crack growth response by two-parameter fracture mechanics", *Materials Science and Engineering: A* vol. **387-389** 2004, 491 –494, 2004. [Online]. Available: `http://www.sciencedirect.com/science/article/pii/S0921509304006100`.

[10] P. Hutař, S. Seitl, and Z. Knésl, ''Effect of constraint on fatigue crack propagation near threshold in medium carbon steel", *Computational Materials Science* vol. **37**, no. 1 2006, 51 –57, 2006. [Online]. Available: `http://www.sciencedirect.com/science/article/pii/S0927025605003575`.

[11] J. Tong, ''T-stress and its implications for crack growth", *Engineering Fracture Mechanics* vol. **69**, no. 12 2002, 1325 –1337, 2002. [Online]. Available: `http://www.sciencedirect.com/science/article/pii/S0013794402000024`.

[12] I. Varfolomeev, M. Luke, and M. Burdack, ''Effect of specimen geometry on fatigue crack growth rates for the railway axle material EA4T", *Engineering Fracture Mechanics* vol. **78**, no. 5 2011, 742 –753, 2011. [Online]. Available: `http://www.sciencedirect.com/science/article/pii/S0013794410004868`.

[13] J. Schijve, ''Fatigue Crack Closure: Observations and Technical Significance", *Mechanics of Fatigue Crack Closure* 1988, J. C. Newman, Jr and W. Elber, Eds., 5–34, 1988.

[14] D. Camas, J. Garcia-Manrique, and A. Gonzalez-Herrera, ''Numerical study of the thickness transition in bi-dimensional specimen cracks", *International Journal of Fatigue* vol. **33**, no. 7 2011, 921 –928, 2011. [Online]. Available: `http://www.sciencedirect.com/science/article/pii/S0142112311000545`.

[15] E. Wolf, ''Fatigue crack closure under cyclic tension", *Engineering Fracture Mechanics* vol. **2**, no. 1 1970, 37 –45, 1970. [Online]. Available: `http://www.sciencedirect.com/science/article/pii/0013794470900287`.

[16] M. Rembeck and A. Sjöblom, "A combined numerical and statistical approach to crack propagation modeling and prediction of crack propagation rates", Master Thesis, Applied Mechanics, Chalmers University of Technology, 2012.

[17] E. Lundström, "Modelling of fatigue crack propagation in inconel 718 under hold time conditions", Licentiate Thesis, Department of Management and Engineering, Linköping University, 2014.

[18] D.L. Ball, J.K Donald, M.A James, and R.J Bucci, "The relationships between crack closure, specimen compliance and 'effective' fatigue crack growth rate", *ICAF 2011 Structural Integrity: Influence of Efficiency and Green Imperatives*, J. Komorowski, Ed., Dordrecht: Springer Netherlands, 2011, pp. 265–276, ISBN: 978-94-007-1664-3.

[19] R. G. Forman and S. R. Mettu, "Behavior of surface and corner cracks subjected to tensile and bending loads in Ti-6Al-4V alloy", NASA, 1990. [Online]. Available: https://ntrs.nasa.gov/search.jsp?R=19910009960.

[20] I. Sen, S. Tamirisakandala, D. Miracle, and U. Ramamurty, "Microstructural effects on the mechanical behavior of B-modified Ti–6Al–4V alloys", *Acta Materialia* vol. **55**, no. 15 2007, 4983 –4993, 2007. [Online]. Available: http://www.sciencedirect.com/science/article/pii/S1359645407003370.

[21] M. Delin, "Comparison of the influence of Kb and C(T) sample on the NASGRO performance for the cast alloys 718, Ti-64 and Ti6242", GKN Aerospace, Trollhättan Sweden, Aug. 8, 2014, VOLS:10199200.

[22] S. Roychowdhury and R. Dodds, "Effect of T-stress on fatigue crack closure in 3-D small-scale yielding", *International Journal of Solids and Structures* vol. **41**, no. 9 2004, 2581 –2606, 2004. [Online]. Available: http://www.sciencedirect.com/science/article/pii/S0020768303006383.

[23] ASTM E112-13, *Standard Test Methods for Determining Average Grain Size*. ASTM International, 2013.

[24] ASTM E930-99, *Standard Test Methods for Estimating the Largest Grain Observed in a Metallographic Section (ALA Grain Size)*. ASTM International, 2015.

[25] S. Eriksson, "Documentation of Inco 718 testmaterial to Themlio, P/N VOLS:10057182 and VOLS:10057578, thickness 72-76 mm", Volvo Aero, Trollhättan Sweden, Dec. 15, 2010, VOLS:10059829.

[26] S. Eriksson, "Ti-64 forging testmaterial for Themelio, P/N VOLS:10057176, thickness 72-78 mm", Volvo Aero, Trollhättan Sweden, Dec. 7, 2010, VOLS:10059825.

[27] ASTM E740/E740M, *Standard Practice for Fracture Testing with Surface-Crack Tension Specimens*. ASTM International, 2015.

[28] K. Walker, C. H. Wang, and J. C. Newman Junior, "Fatigue crack closure due to surface roughness and plastic deformation", *11th International Fatigue Congress*, ser. Advanced Materials Research, vol. 891, Trans Tech Publications, May 2014, pp. 319–324.

[29] M. Andersson, "High strain fatigue crack growth and crack closure", Ph.D. dissertation, Department of Mechanical Engineering, Lund University, Lund, Sweden, 2005.

A da/dN - ΔK plots

A.1 Ti64

A.1.1 $R = 0$

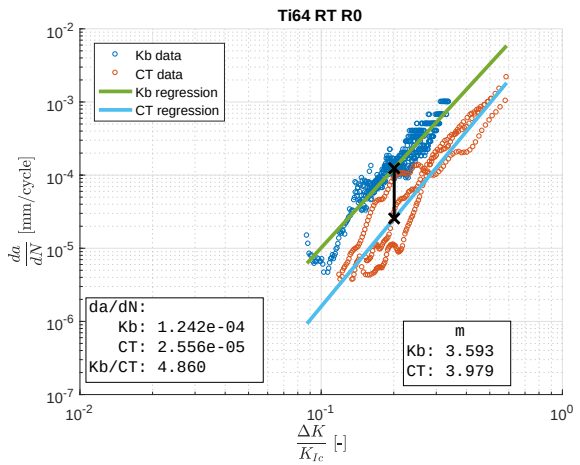

(a) *Fatigue crack growth in Ti64 at RT and* $R = 0$

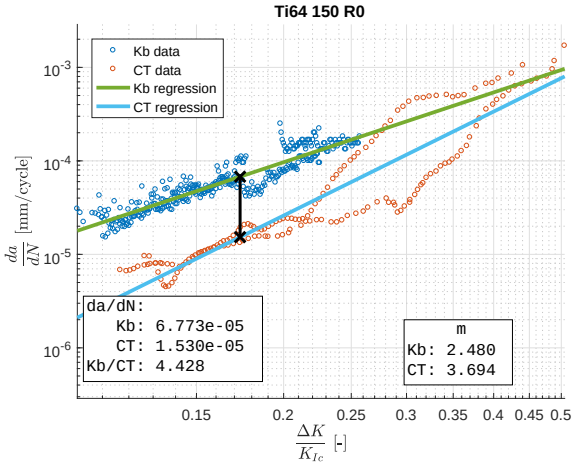

(b) *Fatigue crack growth in Ti64 at 150°C and* $R = 0$

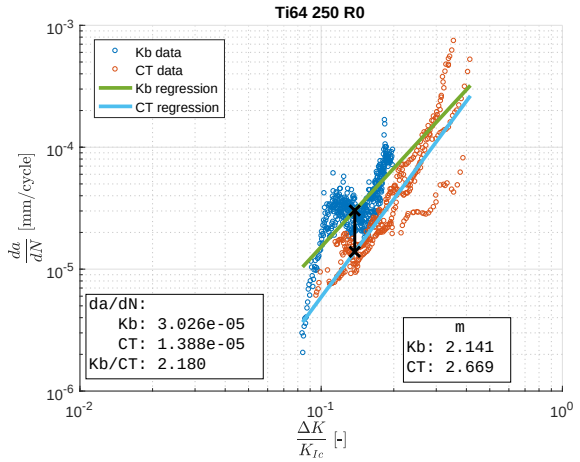

(c) *Fatigue crack growth in Ti64 at 250°C and* $R = 0$

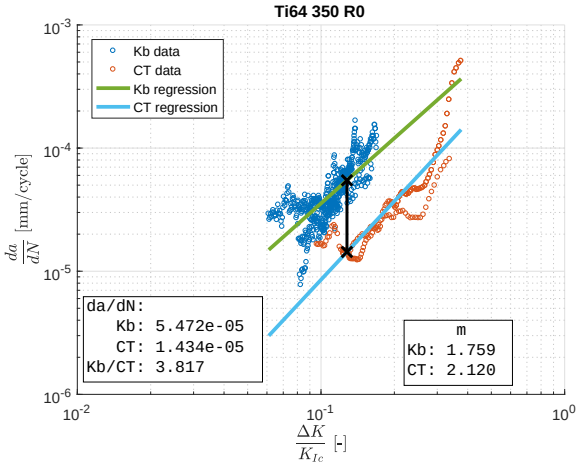

(d) *Fatigue crack growth in Ti64 at 350°C and* $R = 0$

Figure A.1: *Fatigue crack growth in Ti64 at* $R = 0$

A.1.2 $R = 0.5$

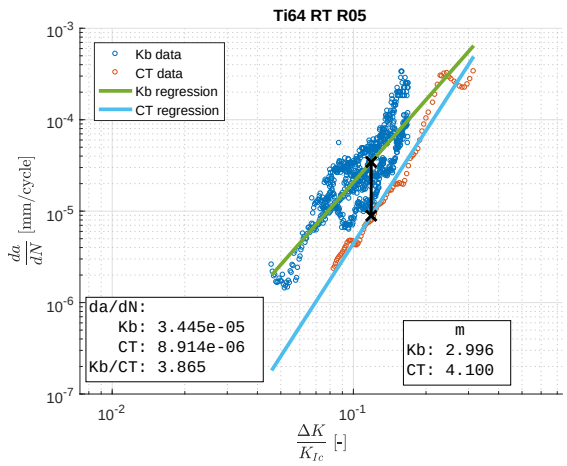

(a) *Fatigue crack growth in Ti64 at RT and* $R = 0.5$

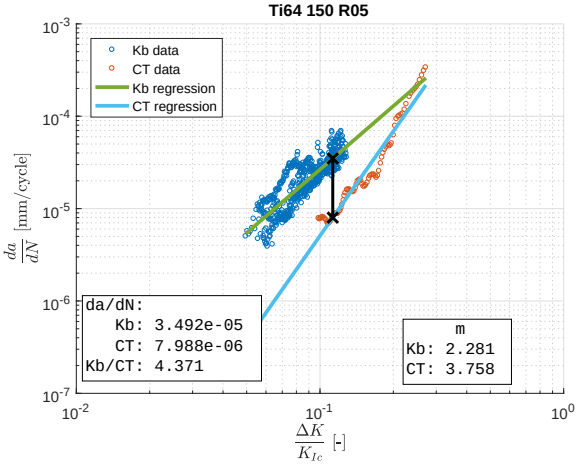

(b) *Fatigue crack growth in Ti64 at 150°C and* $R = 0.5$

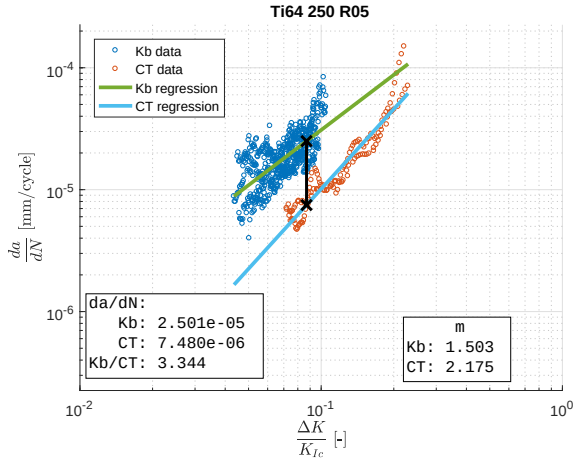

(c) *Fatigue crack growth in Ti64 at 250°C and* $R = 0.5$

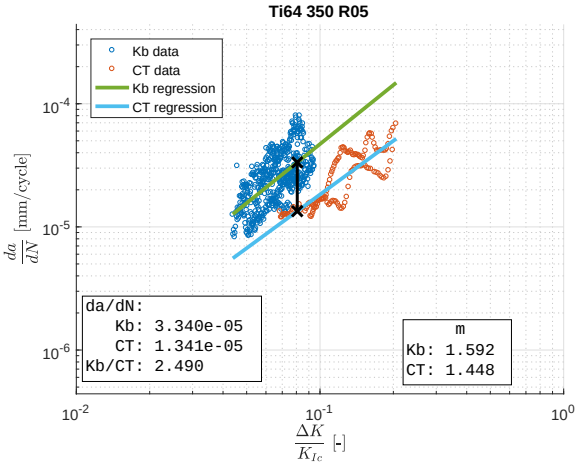

(d) *Fatigue crack growth in Ti64 at 350°C and* $R = 0.5$

Figure A.2: *Fatigue crack growth in Ti64 at* $R = 0.5$

A.2 Ti6242

A.2.1 $R = 0$

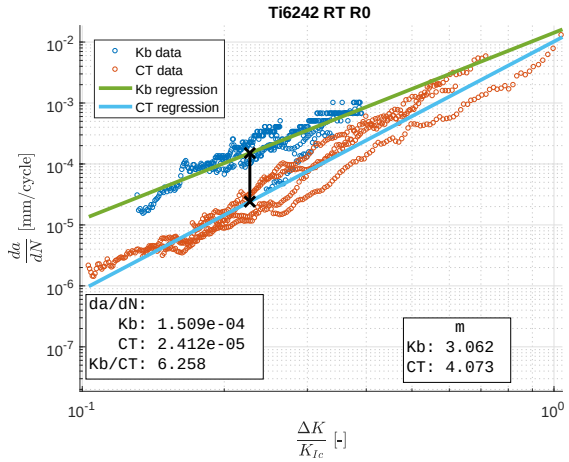

(a) *Fatigue crack growth in Ti6242 at RT and* $R = 0$

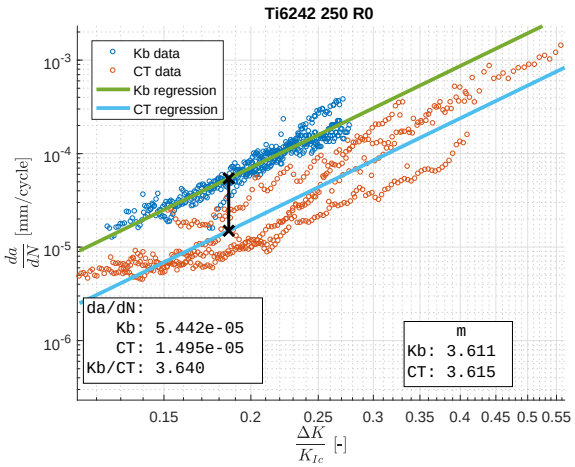

(b) *Fatigue crack growth in Ti6242 at* $250°\mathrm{C}$ *and* $R = 0$

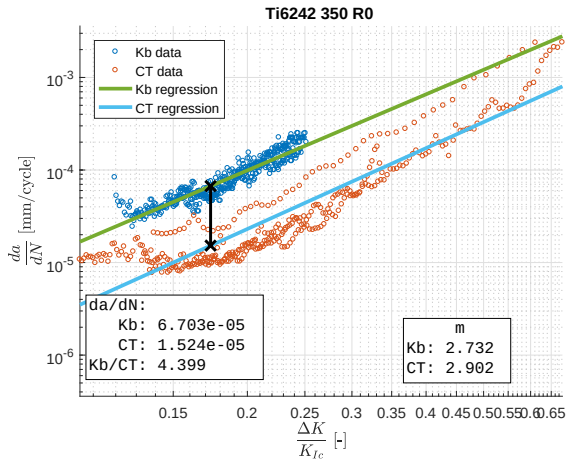

(c) *Fatigue crack growth in Ti6242 at* $350°\mathrm{C}$ *and* $R = 0$

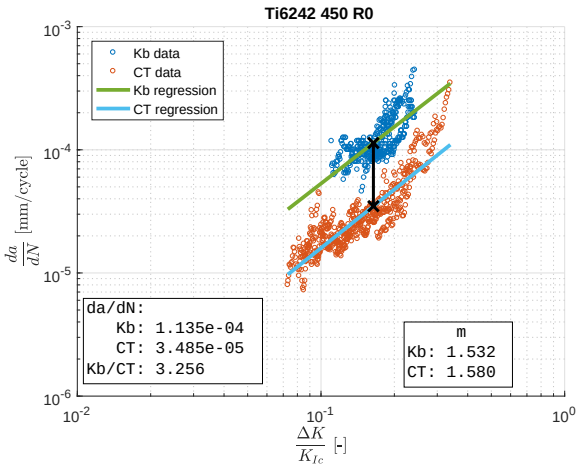

(d) *Fatigue crack growth in Ti6242 at* $450°\mathrm{C}$ *and* $R = 0$

Figure A.3: *Fatigue crack growth in Ti6242 at* $R = 0$

A.2.2 $R = 0.5$

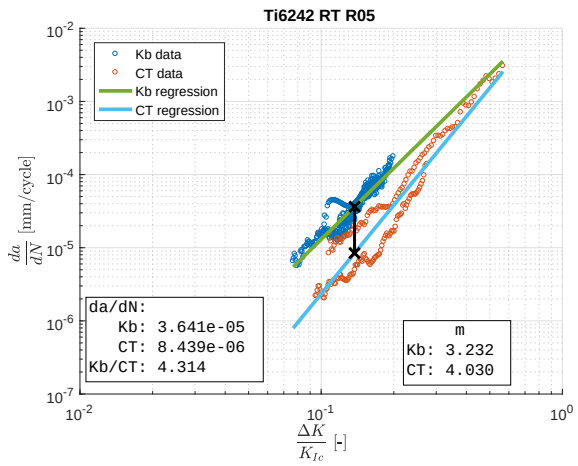

(a) *Fatigue crack growth in Ti6242 at RT and* $R = 0.5$

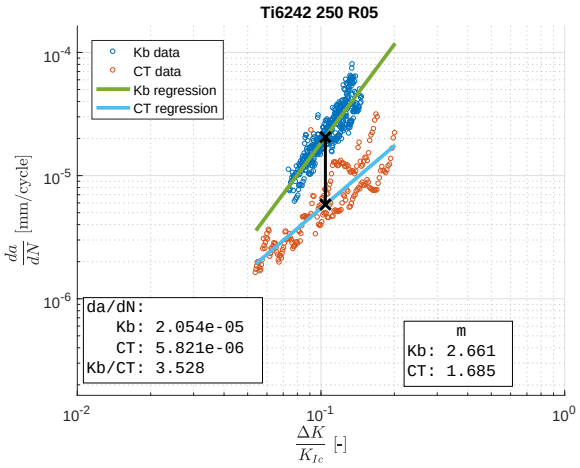

(b) *Fatigue crack growth in Ti6242 at* $250^{\circ}\mathrm{C}$ *and* $R = 0.5$

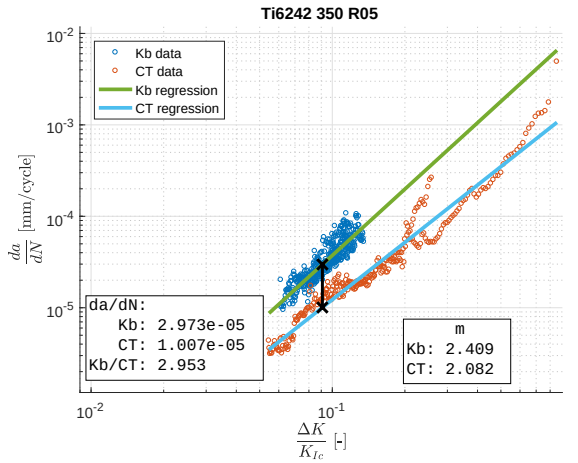

(c) *Fatigue crack growth in Ti6242 at* $350^{\circ}\mathrm{C}$ *and* $R = 0.5$

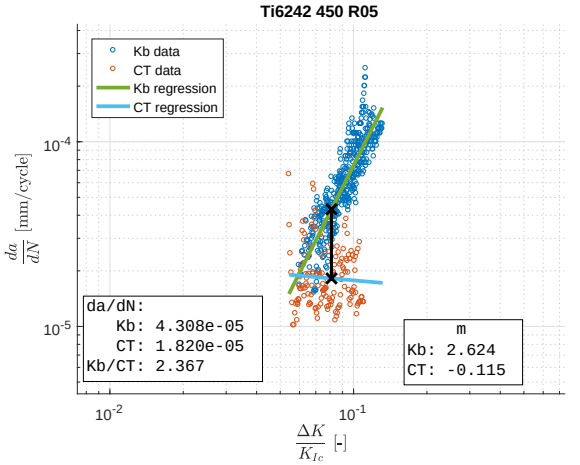

(d) *Fatigue crack growth in Ti6242 at* $450^{\circ}\mathrm{C}$ *and* $R = 0.5$

Figure A.4: *Fatigue crack growth in Ti6242 at* $R = 0.5$

A.3 IN718

A.3.1 $R = 0$

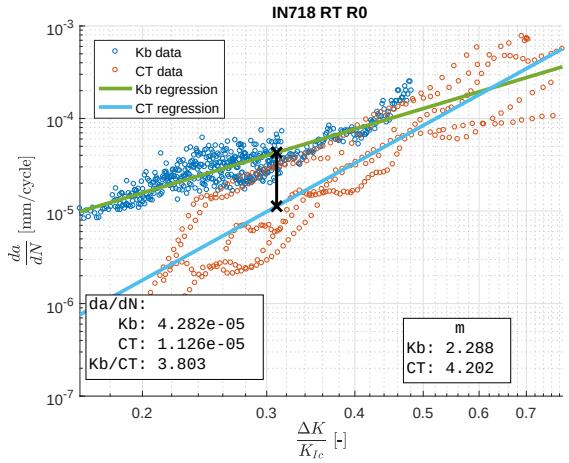

(a) *Fatigue crack growth in IN718 at RT and* $R = 0$

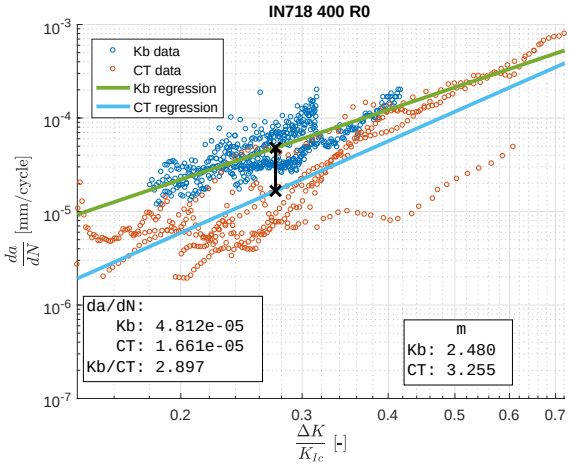

(b) *Fatigue crack growth in IN718 at 400°C and* $R = 0$

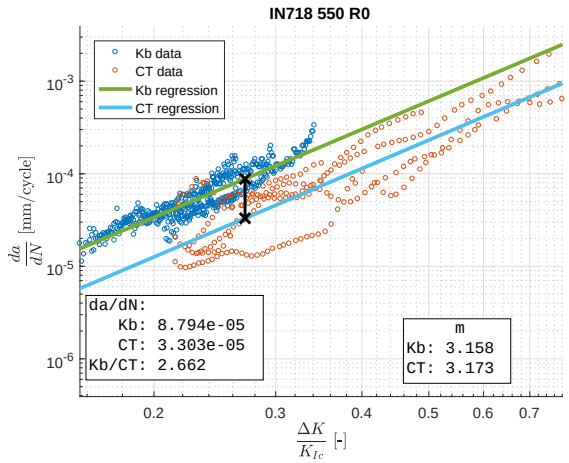

(c) *Fatigue crack growth in IN718 at 550°C and* $R = 0$

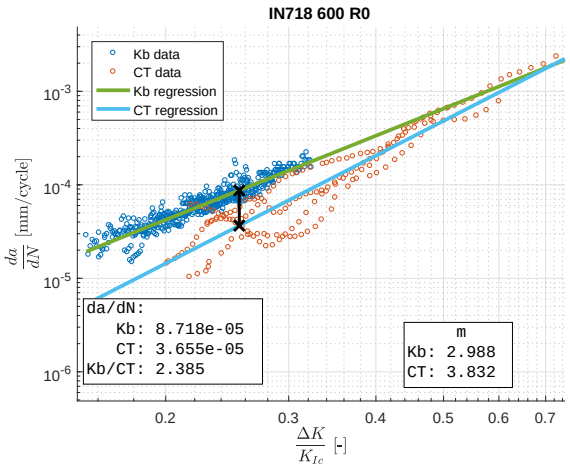

(d) *Fatigue crack growth in IN718 at 600°C and* $R = 0$

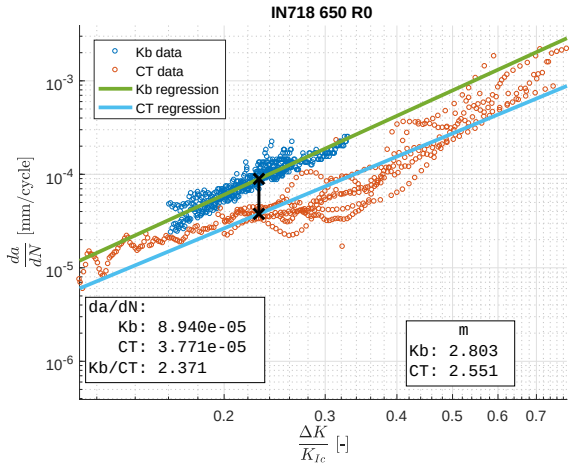

(e) *Fatigue crack growth in IN718 at 650°C and* $R = 0$

Figure A.5: *Fatigue crack growth in IN718 at* $R = 0$

A.3.2 $R = 0.5$

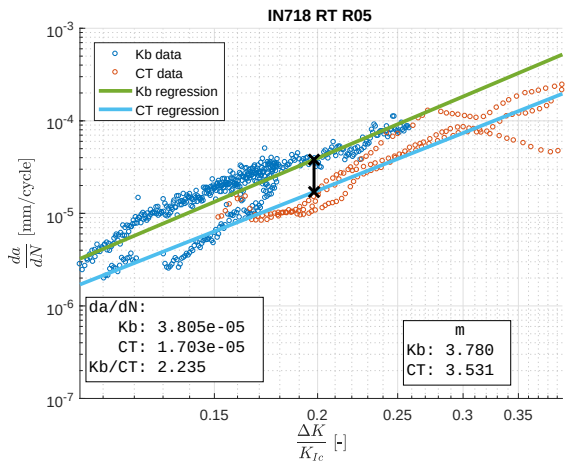

(a) *Fatigue crack growth in IN718 at RT and* $R = 0.5$

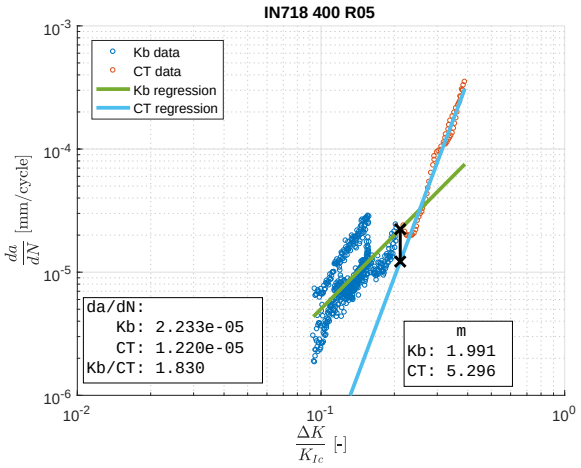

(b) *Fatigue crack growth in IN718 at 400°C and* $R = 0.5$

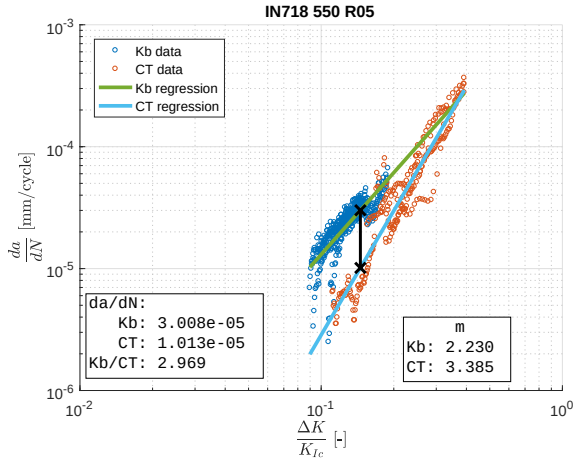

(c) *Fatigue crack growth in IN718 at 550°C and* $R = 0.5$

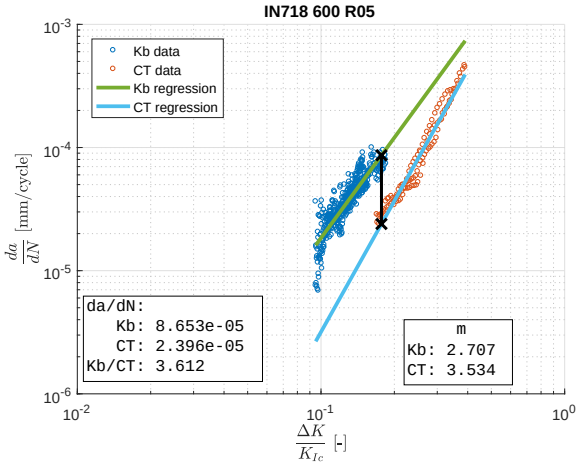

(d) *Fatigue crack growth in IN718 at 600°C and* $R = 0.5$

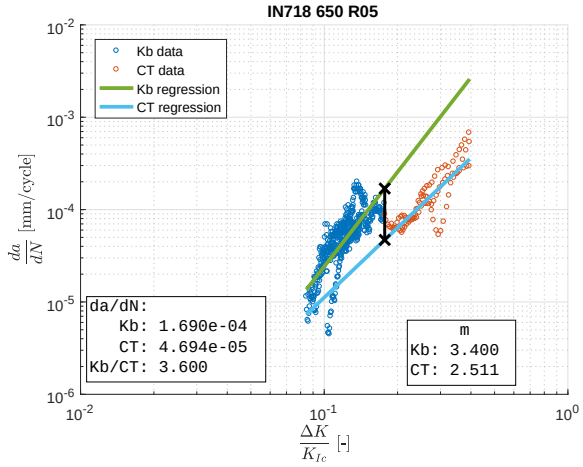

(e) *Fatigue crack growth in IN718 at 650°C and* $R = 0.5$

Figure A.6: *Fatigue crack growth in IN718 at* $R = 0.5$

B Grain size

B.1 Ti-64

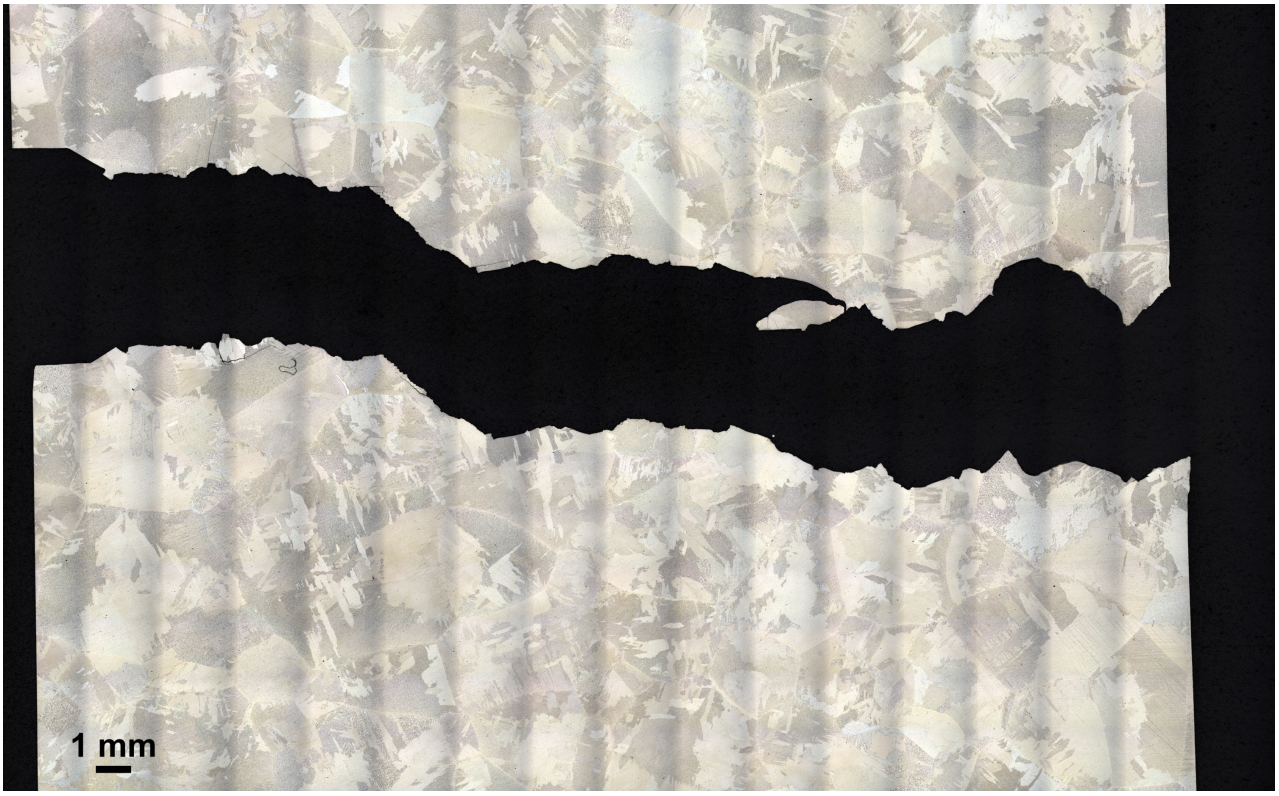

Figure B.1: *Ti-64 grain size sample made from a C(T) specimen. The figure is composed by a number of pictures. The wave pattern is due to bad light conditions for each individual picture.*

Figure B.2: *Ti-64 grain size sample made from a Kb specimen. The figure is composed by a number of pictures.*

Figure B.3: *Ti-64 grain size sample made from a Kb specimen. The figure is composed by a number of pictures.*

B.2 IN-718

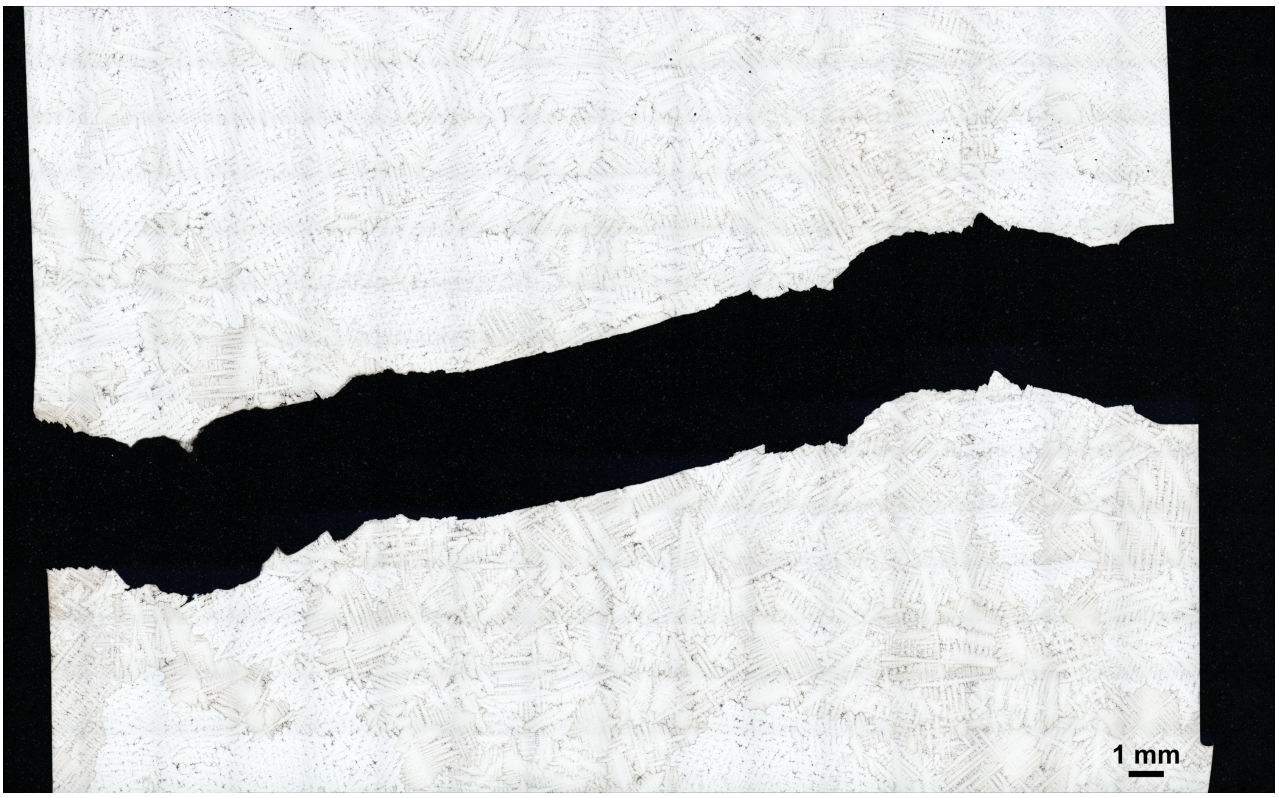

Figure B.4: *IN-718 grain size sample made from a C(T) specimen. The figure is composed by a number of pictures. The wave pattern is due to bad light conditions for each individual picture.*

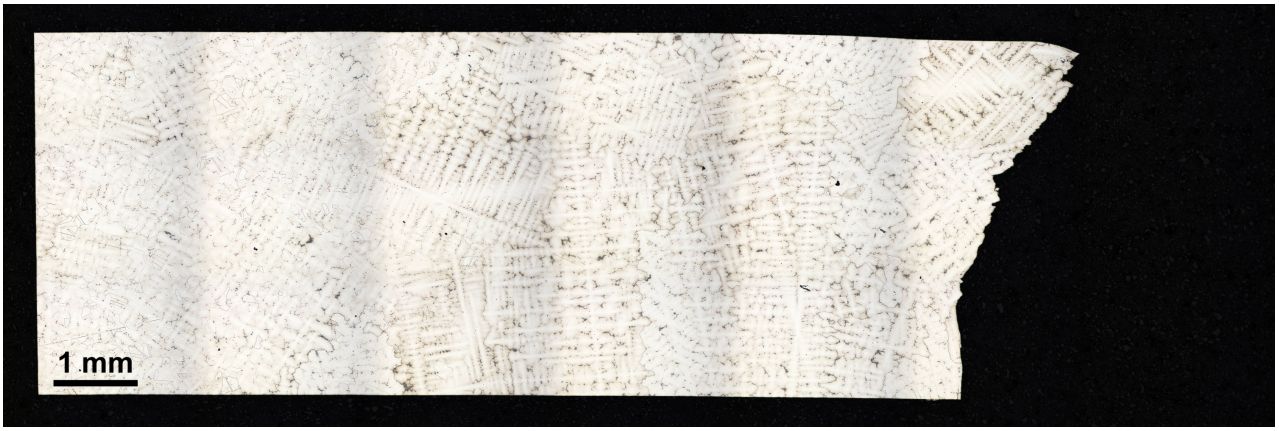

Figure B.5: *IN-718 grain size sample made from a Kb specimen. The figure is composed by a number of pictures. The wave pattern is due to bad light conditions for each individual picture.*

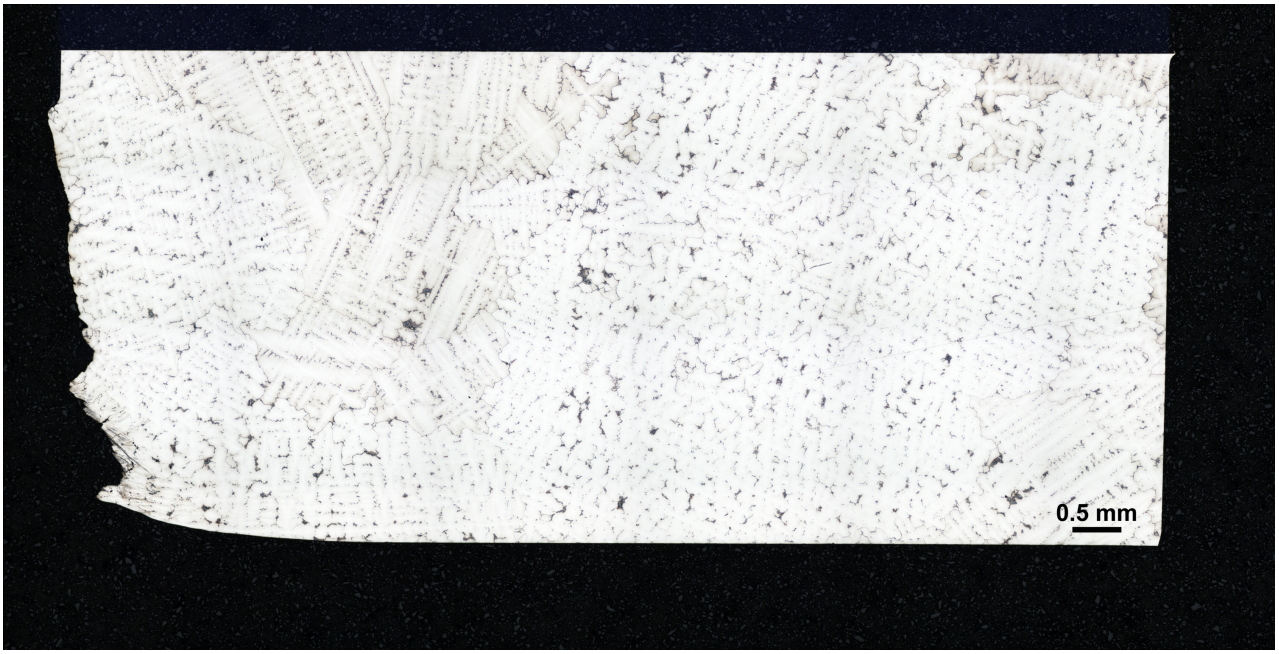

Figure B.6: *IN-718 grain size sample made from a Kb specimen. The figure is composed by a number of pictures.*